Generalized Schlömilch formulas and thermal Casimir effect of a fermionic rectangular box

Zhongyou Mo[1,2] and Junji Jia[1,3,*]
[1]*School of Physics and Technology, Wuhan University, Wuhan, 430072, China*
[2]*Center for Theoretical Physics, Wuhan University, 430072, China*
[3]*Artificial Micro- and Nano-structures, Wuhan University, 430072, China*

(Received 16 May 2018; published 31 July 2018)

Schlömilch's formula is generalized and applied to the thermal Casimir effect of a fermionic field confined to a three-dimensional rectangular box. The analytic expressions of the Casimir energy and Casimir force are derived for arbitrary temperature and edge sizes. The low- and high-temperature limits and finite-temperature cases are considered for the entire parameter space spanned by edge sizes and/or temperature. In the low-temperature limit, it is found that for typical rectangular box, the effective two-dimensional parameter space spanned by the two edge-size ratios can be split into four regions. In one region, all three forces between three pairs of faces are attractive, and in another two regions, the force along the longest edge becomes repulsive, and in the last region the force along both the longest and medium sized edges becomes repulsive. Three forces cannot be made simultaneously repulsive. For the waveguide under low temperature, the Casimir force along the longer side of the waveguide cross section transforms from attractive to repulsive when the aspect ratio of the cross section exceeds a critical value. For the parallel plate scenario under low temperature, our results agree with previous works. For high-temperature limit, it is shown that both the Casimir energy and force approach zero due to the high-temperature suppression of the quantum fluctuation responsible for the Casimir energy. For the finite-temperature case, we separate the parameter space into four subcases (C1–C4) and various edge-size and temperature effects are analyzed. In general, we found that in all cases the Casimir energy is always negative, while the Casimir force at any finite or low temperature can be either repulsive or attractive depending on the sizes of the edges. For the case (C1) that is similar to parallel plates with relatively high temperature, it is found that the Casimir force is always attractive, regardless the change of the plate separation. At the given temperature, the Casimir energy and force densities approach the infinite parallel plate limit even when the plate edge size is two times the plate separation. For the case (C2) that is similar to a waveguide with relatively high temperature, the Casimir force along the longer side of the waveguide cross section transforms from attractive to repulsive when this side exceeds a critical value. This critical point forms a boundary in the parameter space when the shorter edge of the waveguide cross section changes and the boundary values decrease with respect to temperature increase. Case (C3) covers the low-temperature parallel plate, typical rectangular box, and waveguide geometries. For the waveguide case, the force along the waveguide longitude also transforms from attractive to repulsive when the waveguide length exceeds certain critical values. These critical values change with respect to temperature in a nontrivial way. For the typical waveguide case (C4) at low temperature, the Casimir energy density along the longitudinal direction is a constant while force density decreases linearly as the waveguide length increases. Finally, for any fixed temperature, there exists a boundary in the parameter space of edge sizes separating the attractive and repulsive regions. Besides, the Casimir energy for an electromagnetic field confined in a three-dimensional box is also derived.

DOI: 10.1103/PhysRevA.98.012512

I. INTRODUCTION

First proposed in 1948 [1], the Casimir effect has been studied extensively using both experimental and theoretical approaches. In the simplest case, the Casimir effect is known as an attraction (or repulsion) between two parallel conducting plates due to the fluctuations of vacuum energy. Experimentally, it has been observed using different materials, geometries, and measurement setups [2–5]. Theoretically, it is usually studied according to the geometry and boundary conditions, temperature, and nature of fields.

Aside from the usual parallel plates geometry, other geometries such as cylindrical, spherical boundaries, rectangular cavities, and spherical-plate geometries are often studied. In particular, the study of spherical boundaries first by Boyer [6] and later by Milton *et al.* [7] for electromagnetic field showed that the Casimir force could be repulsive too. The theory of Casimir effect for systems with boundaries of real body was established by Lifshitz in Ref. [8], where he also considered the effect of temperature.

Temperature is another important factor influencing the Casimir effect. The thermal Casimir effect was calculated for electromagnetic and/or scalar field confined in rectangular cavities in Refs. [9–13]. Lim and Teo studied the Casimir effect for massless scalar field and electromagnetic field

*junjijia@whu.edu.cn

 ©2018 American Physical Society

[14,15] for piston geometries. Lin and Zhai discussed the finite-temperature Casimir effect in general p-dimensional rectangular cavity [16]. Finite-temperature Casimir effect for electromagnetic field with a boundary of a spherical shell was computed by Balian and Duplantier [17], giving the free energy in low- and high-temperature limits.

The Casimir effect also depends crucially on the nature of the field, i.e., scalar, fermionic, gauge field, and mass of the field. In particular, the fermionic field Casimir effect is considered by a series of papers. The Casimir effect for massless Dirac field confined between two parallel plates was studied by Johnson [18] and Milonni in Ref. [19], where they showed that the Casimir force is attractive as in the case of electromagnetic field. Calculations by Gundersen and Ravndal [20] showed the Casimir force becomes repulsive at sufficiently high temperatures for massless fermions also confined between parallel plates. In this work, many interesting properties such as temperature inversion symmetry, energy-momentum tensor, and fermion condensate were discussed. The Casimir energy for a massless fermionic field confined in a three-dimensional rectangular box at zero temperatures was studied by Seyedzahedi *et al.* [21], showing the Casimir energy is negative as opposed to the case of a three-dimensional sphere considered by Milton [22] where the Casimir energy is positive. Besides, extra dimension corrections for a three-dimensional box with massless fermionic field were considered by Sukamto and Purwanto [23].

In this paper, we extend the above works by study of the thermal Casimir effect at arbitrary temperature for a massless fermionic field confined in a rectangular box. In doing this, we used the generalized Schlömilch's formulas for the evaluation of the frequency summation. We also used this method to study the thermal Casimir effect of an electromagnetic field confined to a three-dimensional rectangular box and found that the resulting Casimir energy in a cube at zero temperature agrees perfectly with previously reported results at low temperature [13].

This paper is organized as follows. In Sec. II, the Schlömilch's formula is briefly introduced and generalized to the cases of double series and triple series. In Sec. III, the generalized Schlömilch's formulas are applied to the thermal Casimir effect of an electromagnetic field confined in a rectangular box. In Sec. IV, the thermal Casimir effect is considered for a massless fermionic field confined in a rectangular box with MIT bag model boundary condition. The general formulas of the Casimir energy and force for arbitrary temperature and edges sizes are derived in this section. Then, in Sec. V the Casimir effect in the entire parameter space spanned by the temperature and three edge sizes is thoroughly studied, in both analytical and numerical ways. Section VI summarizes the findings and outlines potential extensions of the work and other possible applications of the generalized Schlömilch's formula.

II. SCHLÖMILCH'S FORMULA AND ITS GENERALIZATION

A useful formula first discovered by Schlömilch [24,25] and used in many works [26–28] (see [29] for older papers) is the following:

$$\alpha\sum_k \frac{k}{e^{2\alpha k}-1}+\beta\sum_k \frac{k}{e^{2\beta k}-1}=\frac{\alpha+\beta}{24}-\frac{1}{4}, \tag{1}$$

where $\alpha,\beta>0$, $\alpha\beta=\pi^2$, and the sum here and after runs from 1 to infinity until otherwise explicitly specified. A formula derived from Eq. (1), which is also useful by itself, is [29]

$$\sum_k \ln(1-e^{-\alpha k})=\sum_k \ln\left(1-e^{\frac{-4\pi^2 k}{\alpha}}\right)-\frac{\ln\alpha}{2}-\frac{\pi^2}{6\alpha}+\frac{\alpha}{24}+\frac{\ln(2\pi)}{2}. \tag{2}$$

The similarity between the Bose-Einstein distribution and terms in Eq. (1) enables its possible applications in physics, particularly in Casimir effects. It is observable the functions in the sums on the left side of Eq. (1) look like the average energy u_A of a single resonator in Planck's law for the energy spectrum [30]

$$\mathrm{u}(\nu,T)=\frac{8\pi\nu^2}{c^3}u_A=\frac{8\pi\nu^2}{c^3}\frac{h\nu}{e^{h\nu/(k_BT)}-1}, \tag{3}$$

where T is the temperature and k_B is the Boltzmann constant. Because of this, Eqs. (1) and (2) are useful to calculate the internal energy U and free energy F of a one-dimensional linear harmonic oscillators system with discrete frequencies [31]

$$U=\sum_n\left[\frac{\hbar\omega_n}{2}+\frac{\hbar\omega_n}{e^{\hbar\omega_n/(k_BT)}-1}\right], \tag{4}$$

$$F=\sum_n\left[\frac{\hbar\omega_n}{2}+k_BT\ln(1-e^{\hbar\omega_n/(k_BT)})\right]. \tag{5}$$

For a three-dimensional linear harmonic oscillator system, the series in Eqs. (4) and (5) will contain more than one summation. Therefore, the generalizations of Eqs. (1) and (2) to the cases of double series and triple series are necessary for the purpose of application in Casimir effect.

This generalization is done by the technique of contour integral. Consider the following contour integrals, which can be easily shown to be zero since there is no pole inside the contours:

$$\oint G(z)dz=\oint\frac{1}{e^{-uzi}-1}\frac{\sqrt{z^2+m^2}}{e^{\alpha\sqrt{z^2+m^2}}-1}dz=0, \tag{6}$$

$$\oint \tilde{G}(z)dz=\oint\frac{1}{e^{uzi}-1}\frac{\sqrt{z^2+m^2}}{e^{\alpha\sqrt{z^2+m^2}}-1}dz=0, \tag{7}$$

where parameters u,m,α are all positive. The contours are shown in Fig. 1, where ρ is the radius of the small half or quarter circles. The width and height of each contour are specified by points A and B with values

$$\frac{2N\pi}{u}<A<\frac{2(N+1)\pi}{u}\ \text{and}\ \sqrt{m^2+\frac{4N^2\pi^2}{\alpha^2}}<B<\sqrt{m^2+\frac{4(N+1)^2\pi^2}{\alpha^2}}, \tag{8}$$

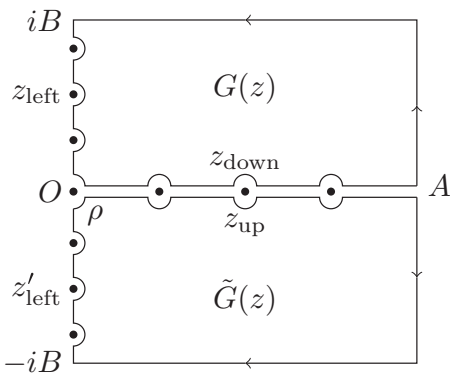

FIG. 1. Contours of integrals (6) (upper contour) and (7) (lower contour) and some of their poles.

where N is some positive integer. In this plot, we also draw some of the poles of $G(z)$ that are relevant to the contour,

$$z_{\text{left}} = i\sqrt{m^2 + \frac{4n^2\pi^2}{\alpha^2}}, \quad z_{\text{down}} = \frac{2n\pi}{u} \quad (n = 1, 2, \ldots, N) \tag{9}$$

and poles of $\tilde{G}(z)$

$$z'_{\text{left}} = -i\sqrt{m^2 + \frac{4n^2\pi^2}{\alpha^2}}, \quad z_{\text{up}} = \frac{2n\pi}{u} \quad (n = 1, 2, \ldots, N). \tag{10}$$

Equations (6) and (7) lead to

$$\begin{aligned}
&\int_\rho^A [G(x) + \tilde{G}(x)]dx + i\int_0^B [G(A + iy) - \tilde{G}(A - iy)]dy \\
&\quad + \int_A^0 [G(x + iB) + \tilde{G}(x - iB)]dx \\
&\quad + i\int_B^\rho [G(iy) - \tilde{G}(-iy)]dy \\
&= i\pi\left\{\frac{1}{2}\text{Res}G(0) - \frac{1}{2}\text{Res}\tilde{G}(0) + \sum_{n=1}^{N}[\text{Res}G(z_{\text{left}}) \right. \\
&\quad \left. + \text{Res}G(z_{\text{down}}) - \text{Res}\tilde{G}(z'_{\text{left}}) - \text{Res}\tilde{G}(z_{\text{up}})]\right\},
\end{aligned} \tag{11}$$

where

$$\begin{aligned}
\text{Res}G(z_{\text{left}}) &= -\text{Res}\tilde{G}(z'_{\text{left}}) \\
&= \frac{i4\pi^2 n^2}{\alpha^3\sqrt{m^2 + 4n^2\pi^2/\alpha^2}(e^{u\sqrt{m^2+4n^2\pi^2/\alpha^2}} - 1)},
\end{aligned} \tag{12}$$

$$\text{Res}G(z_{\text{down}}) = -\text{Res}\tilde{G}(z_{\text{up}}) = \frac{i\sqrt{m^2 + 4n^2\pi^2/u^2}/u}{e^{\alpha\sqrt{m^2+4n^2\pi^2/u^2}} - 1}, \tag{13}$$

$$\text{Res}G(0) = -\text{Res}\tilde{G}(0) = \frac{im}{u(e^{\alpha m} - 1)}. \tag{14}$$

It is not hard to see that

$$\lim_{x\text{or}y\to\infty} G(x + iy) = \lim_{x\text{or}y\to\infty} \tilde{G}(x - iy) = 0, \tag{15}$$

and the second and third integrals in Eq. (11) vanish when A and B, equivalently N, go to infinity. Then, letting $u = 2\pi/\theta$, Eq. (11) can be recast into the equality

$$\begin{aligned}
&\sum_n \frac{\sqrt{\theta^2 n^2 + m^2}}{e^{\alpha\sqrt{\theta^2 n^2 + m^2}} - 1} \\
&= -\frac{8\pi^3}{\theta\alpha^3}\sum_n \frac{n^2}{\sqrt{\frac{4\pi^2 n^2}{\alpha^2} + m^2}\left(e^{\frac{2\pi}{\theta}\sqrt{\frac{4\pi^2 n^2}{\alpha^2} + m^2}} - 1\right)} \\
&\quad - \frac{m}{2(e^{\alpha m} - 1)} \\
&\quad + \frac{1}{\theta}\left(\int_0^\infty \frac{\sqrt{x^2 + m^2}}{e^{\alpha\sqrt{x^2+m^2}} - 1}dx + \int_m^\infty \frac{\sqrt{y^2 - m^2}}{e^{\frac{2\pi}{\theta}y} - 1}dy\right).
\end{aligned} \tag{16}$$

Note that this equation implies Eq. (1). This can be seen by setting $\theta = 1$ and $m = 0$ in Eq. (16) and carrying out the integral using formula [32]

$$\int_0^\infty \frac{x^{s-1}e^{-ax}}{1 - e^{-x}}dx = \Gamma(s)\zeta(s, a), \tag{17}$$

where $\Gamma(s)$ is gamma function and

$$\zeta(s, a) = \sum_{n=0} \frac{1}{(n + a)^s} \tag{18}$$

is the Hurwitz zeta function and $\zeta(s, 1) \equiv \zeta(s)$ is the Riemann zeta function.

To generalize Eq. (16) to the case of double series, we replace m in it by σm and then sum over m. One then obtains

$$\begin{aligned}
\sum_m\sum_n \frac{\sqrt{\theta^2 n^2 + \sigma^2 m^2}}{e^{\sqrt{\theta^2 n^2 + \sigma^2 m^2}} - 1} &= -\frac{8\pi^3}{\theta}\sum_m\sum_n \frac{n^2}{\sqrt{4\pi^2 n^2 + \sigma^2 m^2}\left(e^{\frac{2\pi}{\theta}\sqrt{4\pi^2 n^2 + \sigma^2 m^2}} - 1\right)} - \sum_m \frac{\sigma m}{2(e^{\sigma m} - 1)} \\
&\quad + \frac{1}{\theta}\sum_m \int_0^\infty \frac{\sqrt{x^2 + \sigma^2 m^2}}{e^{\sqrt{x^2+\sigma^2 m^2}} - 1}dx + \frac{1}{\theta}\sum_m \int_{\sigma m}^\infty \frac{\sqrt{y^2 - \sigma^2 m^2}}{e^{\frac{2\pi}{\theta}y} - 1}dy,
\end{aligned} \tag{19}$$

where $\theta, \sigma > 0$. The first and second terms on the right side will be kept. The third term can be calculated again using Eq. (16), and then for some terms using

$$\frac{1}{e^y - 1} = \sum_n e^{-yn}, \tag{20}$$

and lastly using the definition of Bessel function of an imaginary argument [33]

$$K_\nu(z) = \frac{(z/2)^\nu \Gamma(1/2)}{\Gamma(\nu+1/2)} \int_1^\infty e^{-zt}(t^2-1)^{\nu-1/2} dt \tag{21}$$

and the formula (17). For the fourth term, we only need to use Eqs. (20) and (21). Combining all, the final result of the double series (19) is given by

$$\sum_{m,n} \frac{\sqrt{\theta^2 n^2 + \sigma^2 m^2}}{e^{\sqrt{\theta^2 n^2+\sigma^2 m^2}} - 1} = -\frac{8\pi^3}{\theta} \sum_{m,n} \frac{n^2}{\sqrt{4\pi^2 n^2 + \sigma^2 m^2}\left(e^{\frac{2\pi}{\theta}\sqrt{4\pi^2 n^2+\sigma^2 m^2}} - 1\right)} - \frac{\sigma}{2} \sum_m \frac{m}{e^{\sigma m} - 1}$$
$$+ \frac{1}{\theta}\left[-\frac{8\pi^3}{\sigma} Y_0\left(\frac{2\pi}{\sigma}\right) - \frac{\zeta(2)}{2} + \frac{\pi\zeta(3)}{\sigma} + \frac{\zeta(3)\sigma^2}{16\pi^2}\right] + \frac{\sigma}{2\pi} Y_1\left(\frac{\sigma}{\theta}\right), \tag{22}$$

where functions $Y_0(x)$ and $Y_1(x)$ are

$$Y_0(x) = \sum_{m,n} m^2 K_0(2\pi mnx), \quad Y_1(x) = \sum_{m,n} \frac{m}{n} K_1(2\pi mnx). \tag{23}$$

Equation (2) can also be generalized to the cases of double series. Letting $\theta = \alpha/a$ and $\sigma = \alpha/b$, then dividing Eq. (22) by α, indefinitely integrating both sides with respect to α, and using the property of Bessel function [33]

$$\left(\frac{d}{zdz}\right)^i [z^\nu K_\nu(z)] = (-1)^i z^{\nu-i} K_{\nu-i}(z) \tag{24}$$

at $i = 1$ for Y_0 yields

$$\sum_{n,m} \ln\left(1 - e^{-\alpha\sqrt{\frac{n^2}{a^2}+\frac{m^2}{b^2}}}\right) = Z_2\left(a, b, \frac{\alpha}{2\pi}\right) - \frac{1}{2} Z_1\left(\frac{\alpha}{2\pi b}\right) + a\left[\frac{\zeta(2)}{2\alpha} - \frac{\pi\zeta(3)b}{2\alpha^2} + \frac{\zeta(3)\alpha}{16\pi^2 b^2} - \frac{2\pi}{\alpha} Y_1\left(\frac{2\pi b}{\alpha}\right)\right]$$
$$+ \frac{\alpha}{2\pi b} Y_1\left(\frac{a}{b}\right) + Q(a, b), \tag{25}$$

where $Z_1(x)$ and $Z_2(x, y, z)$ are

$$Z_1(x) = \sum_m \ln(1 - e^{-2\pi mx}), \quad Z_2(x, y, z) = \sum_{n,m} \ln(1 - e^{-2\pi x\sqrt{n^2/y^2+m^2/z^2}}) \tag{26}$$

and the integral constant $Q(a, b)$ is

$$Q(a, b) = \frac{1}{2} Z_1\left(\frac{a}{b}\right) - \frac{\zeta(2)}{4\pi} + \frac{\zeta(3)b}{8\pi a} - \frac{\zeta(3)a^2}{8\pi b^2} + Y_1\left(\frac{b}{a}\right) - \frac{a}{b} Y_1\left(\frac{a}{b}\right). \tag{27}$$

Note that the $Z_1(\alpha/(2\pi b))$ in Eq. (25) can be calculated by Eq. (2).

Finally, let us generalize Eqs. (1) and (2) to the triple series case. Applying Eqs. (16), (22), (20), and (21) to the triple series, and performing the summation in the order of n, j, and m, yields its result

$$\sum_{n,m,j} \frac{\sqrt{\theta^2 n^2 + \sigma^2 m^2 + \gamma^2 j^2}}{e^{\sqrt{\theta^2 n^2+\sigma^2 m^2+\gamma^2 j^2}} - 1}$$
$$= -\frac{8\pi^3}{\theta} \sum_{k,m,j} \frac{k^2}{\sqrt{4\pi^2 k^2 + \sigma^2 m^2 + \gamma^2 j^2}\left(e^{\frac{2\pi}{\theta}\sqrt{4\pi^2 k^2+\sigma^2 m^2+\gamma^2 j^2}} - 1\right)}$$
$$- \sum_{m,j} \frac{\sqrt{\sigma^2 m^2 + \gamma^2 j^2}}{2\left(e^{\sqrt{\sigma^2 m^2+\gamma^2 j^2}} - 1\right)} + \frac{1}{\theta}\left\{\frac{-8\pi^3}{\gamma} \sum_{m,k,n} k^2 K_0\left(\frac{2\pi\sigma n}{\gamma}\sqrt{m^2 + \frac{4k^2\pi^2}{\sigma^2}}\right) + \left[\frac{\zeta(2)}{4} - \frac{\pi\zeta(3)}{2\sigma} - \frac{\zeta(3)\sigma^2}{32\pi^2} + \frac{4\pi^3}{\sigma} X_0\left(\frac{2\pi}{\sigma}\right)\right]\right.$$
$$\left. + \frac{1}{\gamma}\left[\frac{-\pi\zeta(3)}{2} + \frac{3\pi\zeta(4)}{\sigma} + \frac{\zeta(4)\sigma^3}{16\pi^3} - 4\pi^4\left(\frac{2}{\pi\sigma}\right)^{\frac{1}{2}} \sum_{k,n}\left(\frac{k^5}{n}\right)^{\frac{1}{2}} K_{\frac{1}{2}}\left(\frac{4\pi^2 kn}{\sigma}\right)\right] + \frac{\gamma^{\frac{1}{2}}\sigma^{\frac{3}{2}}}{4\pi} Y_{\frac{3}{2}}\left(\frac{\sigma}{\gamma}\right)\right\} + \frac{1}{2\pi} V_1\left(\frac{1}{\theta}, \frac{1}{\sigma}, \frac{1}{\gamma}\right), \tag{28}$$

where variables $\theta, \sigma, \gamma > 0$, and $Y_{3/2}(x)$, $V_1(x, y, z)$ are

$$Y_{\frac{3}{2}}(x) = \sum_{m,n}\left(\frac{m}{n}\right)^{\frac{3}{2}} K_{\frac{3}{2}}(2\pi mnx), \quad V_1(x, y, z) = \sum_{k,m,n} \frac{\sqrt{m^2/y^2 + k^2/z^2}}{n} K_1(2\pi nx\sqrt{m^2/y^2 + k^2/z^2}). \tag{29}$$

Furthermore, in Eq. (28) letting $\theta = \alpha/a$, $\sigma = \alpha/b$, and $\gamma = \alpha/c$, then dividing by α and indefinitely integrating both sides with respect to α yields

$$\sum_{n,m,j} \ln\left(1 - e^{-\alpha\sqrt{\frac{n^2}{a^2}+\frac{m^2}{b^2}+\frac{j^2}{c^2}}}\right) = Z_3\left(a, b, c, \frac{\alpha}{2\pi}\right) - \frac{1}{2}Z_2\left(\frac{\alpha}{2\pi}, b, c\right) + a\left\{-V_1\left(c, b, \frac{\alpha}{2\pi}\right)\right.$$
$$+\left[\frac{-\zeta(2)}{4\alpha} + \frac{\pi\zeta(3)b}{4\alpha^2} - \frac{\zeta(3)\alpha}{32\pi^2b^2} + \frac{\pi}{\alpha}Y_1\left(\frac{2\pi b}{\alpha}\right)\right] + c\left[\frac{\pi\zeta(3)}{4\alpha^2} - \frac{\pi\zeta(4)b}{\alpha^3} + \frac{\zeta(4)\alpha}{16\pi^3b^3} - \pi\left(\frac{2\pi}{b\alpha^3}\right)^{1/2}Y_{\frac{3}{2}}\left(\frac{2\pi b}{\alpha}\right)\right]$$
$$\left. + \frac{\alpha}{4\pi c^{1/2}b^{3/2}}Y_{\frac{3}{2}}\left(\frac{c}{b}\right)\right\} + \frac{\alpha}{2\pi}V_1(a, b, c) + N(a, b, c), \tag{30}$$

where $Z_2(x, y, z)$ was defined in Eq. (26), and function $Z_3(x, y, z, t)$ and the integral constant $N(a, b, c)$ are, respectively,

$$Z_3(x, y, z, t) = \sum_{n,m,j} \ln\left(1 - e^{-2\pi x\sqrt{n^2/y^2+m^2/z^2+j^2/t^2}}\right), \tag{31}$$

$$N(a, b, c) = \frac{1}{2}Z_2(a, b, c) + a[V_1(c, a, b) - V_1(a, b, c)] + \frac{\zeta(2)}{8\pi} - \frac{1}{2}Y_1\left(\frac{b}{a}\right) + \left[\frac{\zeta(3)a^2}{16\pi b^2} - \frac{\zeta(3)b}{16\pi a} - \frac{\zeta(3)c}{16\pi a}\right]$$
$$+ c\left[\frac{\zeta(4)b}{8\pi^2a^2} - \frac{\zeta(4)a^2}{8\pi^2b^3}\right] + \frac{c}{2b^{1/2}a^{1/2}}Y_{\frac{3}{2}}\left(\frac{b}{a}\right) - \frac{a^2}{2c^{1/2}b^{3/2}}Y_{\frac{3}{2}}\left(\frac{c}{b}\right). \tag{32}$$

Equations (28) and (30) are the generalizations of Eqs. (1) and (2) to the triple series case. In addition, when the sign in the ln function in Eq. (30) is changed from minus to plus, one can reach the formula

$$\sum_{n,m,j} \ln(1 + e^{-\alpha\sqrt{\frac{n^2}{a^2}+\frac{m^2}{b^2}+\frac{j^2}{c^2}}}) = Z_3\left(\frac{\alpha}{\pi}, a, b, c\right) - Z_3\left(\frac{\alpha}{2\pi}, a, b, c\right)$$
$$= \frac{7\pi\zeta(4)abc}{8\alpha^3} + \alpha\left[\frac{\zeta(4)ac}{16\pi^3b^3} + \frac{a}{4\pi b^{3/2}c^{1/2}}Y_{\frac{3}{2}}\left(\frac{c}{b}\right) + \frac{1}{2\pi}V_1(a, b, c)\right] + Z_3\left(a, b, c, \frac{\alpha}{\pi}\right) - Z_3\left(a, b, c, \frac{\alpha}{2\pi}\right)$$
$$+ aV_1\left(c, b, \frac{\alpha}{2\pi}\right) - aV_1\left(c, b, \frac{\alpha}{\pi}\right) + ac\pi\left(\frac{2\pi}{b\alpha^3}\right)^{1/2}Y_{\frac{3}{2}}\left(\frac{2\pi b}{\alpha}\right) - \frac{ac\pi}{2}\left(\frac{\pi}{b\alpha^3}\right)^{1/2}Y_{\frac{3}{2}}\left(\frac{\pi b}{\alpha}\right)$$
$$+ \frac{\zeta(2)a}{8\alpha} - \frac{3\pi\zeta(3)ab}{16\alpha^2} - \frac{3\pi\zeta(3)ac}{16\alpha^2} - \frac{\zeta(3)a\alpha}{32\pi^2b^2} + \frac{1}{2}Z_2\left(\frac{\alpha}{2\pi}, b, c\right) - \frac{1}{2}Z_2\left(\frac{\alpha}{\pi}, b, c\right) + \frac{a\pi}{2\alpha}Y_1\left(\frac{\pi b}{\alpha}\right) - \frac{a\pi}{\alpha}Y_1\left(\frac{2\pi b}{\alpha}\right), \tag{33}$$

which will be useful for the calculation of fermionic field Casimir effect.

III. THERMAL CASIMIR EFFECT OF ELECTROMAGNETIC FIELD IN A RECTANGULAR BOX

Geyer *et al.* [13] studied the Casimir effect of electromagnetic field in ideal metal rectangular boxes at finite temperature. They used the Abel-Plana formula to calculate the nonrenormalized thermal correction term $\Delta_T F_0$ in the renormalized free energy F^{phys} of the electromagnetic field. In this section, we calculate F^{phys} using the generalized Schlömilch's formula developed in Eq. (30) for arbitrary edge sizes and temperature.

The renormalized free energy of electromagnetic field confined in a three-dimensional box is given by [13]

$$F^{\text{phys}}(a, b, c, T) = E_0^{\text{ren}}(a, b, c) + \Delta_T F_0(a, b, c, T) - F_{\text{bb}}(a, b, c, T) - \alpha_1^{el}T^3 - \alpha_2^{el}T^2, \tag{34}$$

where a, b, c are the edge sizes of the box, T is the temperature, and $E_0^{\text{ren}}(a, b, c)$ is the renormalized free energy at zero temperature. $\Delta_T F_0(a, b, c, T)$ is the nonrenormalized thermal correction

$$\Delta_T F_0(a, b, c, T) = T\left[\sum_{n,m} \ln\left(1 - e^{-\frac{\omega_{nm0}}{T}}\right) + \sum_{n,j} \ln(1 - e^{-\frac{\omega_{n0j}}{T}}) + \sum_{m,j} \ln\left(1 - e^{-\frac{\omega_{0mj}}{T}}\right) + 2\sum_{n,m,j} \ln(1 - e^{-\frac{\omega_{nmj}}{T}})\right], \tag{35}$$

where

$$\omega_{nmj} = \pi\sqrt{\frac{n^2}{a^2} + \frac{m^2}{b^2} + \frac{j^2}{c^2}}, \quad n, m, j = 1, 2, \ldots \tag{36}$$

are frequencies, and

$$F_{\text{bb}}(a, b, c, T) = -\frac{\pi^2T^4abc}{45} \tag{37}$$

is the free energy of the black-body radiation. Note in Eq. (35) and throughout this paper, the natural units $\hbar = c = k_B = 1$ are used. Finally, α_1^{el} and α_2^{el} are coefficients of two renormalization terms which should cancel the corresponding terms in

$\Delta_T F_0(a,b,c,T)$ to prevent possible high-temperature divergence that can contribute to the Casimir force.

The renormalized free energy at zero temperature $E_0^{\rm ren}(a,b,c)$ can be calculated using the Abel-Plana formula [34,35] and Epstein zeta function [35]. Starting from the definition of the nonrenormalized zero-temperature free energy $E_0(a,b,c)$,

$$E_0(a,b,c) = \frac{1}{2}\left(2\sum_{n,m,j}\omega_{nmj} + \sum_{n,m}\omega_{nm} + \sum_{n,j}\omega_{nj} + \sum_{m,j}\omega_{mj}\right), \tag{38}$$

one can use the Abel-Plana formula [35]

$$\sum_{n=0} g(n) - \int_0^\infty g(t)dt = \frac{g(0)}{2} + i\int_0^\infty \frac{g(it)-g(-it)}{e^{2\pi t}-1}dt, \tag{39}$$

where $g(z)$ is any analytic function in the right half-plane to perform the summation in Eq. (38) in the order of n, j, and m. This allows us to separate its infinite parts to obtain the finite renormalized free energy at zero temperature $E_0^{\rm ren}(a,b,c)$ as

$$E_0^{\rm ren}(a,b,c) = -a\left[\frac{\zeta(4)c}{8\pi^2 b^3} + \frac{\zeta(3)}{16\pi c^2} + \frac{1}{2b^{3/2}c^{1/2}}Y_{\frac{3}{2}}\left(\frac{c}{b}\right)\right] + \frac{\pi}{48}\left(\frac{1}{b}+\frac{1}{c}\right) - \left[V_1(a,b,c) + \frac{1}{2b}Y_1\left(\frac{a}{b}\right) + \frac{1}{2c}Y_1\left(\frac{a}{c}\right)\right], \tag{40}$$

where $Y_{3/2}(x)$ and $V_1(x,y,z)$ were defined in Eq. (29), and $Y_1(x)$ was defined in Eq. (23).

For the computation of the nonrenormalized thermal correction $\Delta_T F_0(a,b,c,T)$, our approach is different from the Abel-Plana formula method used by Ref. [13]. Instead, in this paper we calculate it using the generalized Schlömilch's formula obtained in Sec. II. Applying Eqs. (30), (25), and (2) to Eq. (35), the analytical form of $\Delta_T F_0(a,b,c,T)$ can be obtained as

$$\Delta_T F_0(a,b,c,T) = -\frac{T\ln T}{2} + T F_1(a,b,c) + F_2(a,b,c,T) - E_0^{\rm ren}(a,b,c) - \frac{2\zeta(4)abc}{\pi^2}T^4 + \frac{\pi(a+b+c)}{12}T^2, \tag{41}$$

where

$$F_1(a,b,c) = \frac{\zeta(4)bc}{4\pi^2 a^2} - a^2\left[\frac{\zeta(4)c}{4\pi^2 b^3} + \frac{\zeta(3)}{8\pi c^2} + \frac{1}{b^{3/2}c^{1/2}}Y_{\frac{3}{2}}\left(\frac{c}{b}\right)\right] + \left[Z_2(a,b,c) + \frac{1}{2}Z_1\left(\frac{a}{b}\right) + \frac{1}{2}Z_1\left(\frac{a}{c}\right) + Y_1\left(\frac{c}{a}\right)\right] - \left[2aV_1(a,b,c) + \frac{a}{b}Y_1\left(\frac{a}{b}\right) + \frac{a}{c}Y_1\left(\frac{a}{c}\right)\right] + 2aV_1(c,b,a) + \frac{c}{\sqrt{ab}}Y_{\frac{3}{2}}\left(\frac{b}{a}\right) - \frac{\ln(bc)}{4} - \frac{\zeta(2)}{4\pi} - \frac{\ln 2}{2}, \tag{42}$$

$$F_2(a,b,c,T) = T\left\{\left[2Z_3\left(a,b,c,\frac{1}{2T}\right) + Z_2\left(a,b,\frac{1}{2T}\right) + Z_2\left(a,c,\frac{1}{2T}\right) - \frac{1}{2}Z_1(2Tb) - \frac{1}{2}Z_1(2Tc)\right] - a\left[2V_1\left(c,b,\frac{1}{2T}\right) + 2c\left(\frac{2T^3}{b}\right)^{1/2}Y_{\frac{3}{2}}(2bT) + 2TY_1(2cT)\right]\right\}. \tag{43}$$

Equation (41) implies that in Eq. (34)

$$\alpha_1^{el} = 0, \quad \alpha_2^{el} = \pi(a+b+c)/12. \tag{44}$$

Equation (44) agrees with Ref. [13] which computed the high-temperature limit of the Casimir energy.

Substituting Eq. (41) into the renormalized free energy (34), the final Casimir energy of electromagnetic field in a three-dimensional rectangular box at finite temperature is finally written as

$$F^{\rm phys}(a,b,c,T) = -\frac{T\ln T}{2} + T F_1(a,b,c) + F_2(a,b,c,T). \tag{45}$$

In order to compare with previous works, we computed the high- and low-temperature limits of (45). At high temperature, we can show in Appendix B that the last term $F_2(a,b,c,T)$ in Eq. (45) approaches zero. Therefore, the Casimir energy becomes

$$F^{\rm phys}(a,b,c,T\to\infty) = -(T\ln T)/2 + T F_1(a,b,c). \tag{46}$$

The first term here is geometry independent and therefore does not contribute to the electromagnetic Casimir force. Moreover, because it is negative and divergent at infinite temperature, this term should be subtracted in order to get a physically meaningful Casimir energy. Finally, we have

$$F^{\rm phys}(a,b,c,T\to\infty) = T F_1(a,b,c). \tag{47}$$

This shows that at high temperature, the temperature dependence of the Casimir energy is particularly simple, while the edge-size dependence is solely through the term $F_1(a,b,c)$.

In the low-temperature limit, we can show that the entire $\Delta_T F_0(a,b,c,T)$ in Eq. (35) goes zero [see the steps from Eq. (B2) to Eq. (B1)]. Therefore, using definition (34), the renormalized free energy in low temperature becomes $E_0^{\rm ren}(a,b,c)$ given in Eq. (40):

$$F^{\rm phys}(a,b,c,T\to 0) = E_0^{\rm ren}(a,b,c). \tag{48}$$

If one is interested in the electromagnetic Casimir energy of a cube at zero temperature, then setting $a=b=c$ in Eq. (40)

produces numerically

$$F^{\rm phys}(a,a,a,T\to 0)=E_0^{\rm ren}(a,a,a)=\frac{0.0917}{a}, \quad (49)$$

and therefore an attractive force between opposite faces of the cube. Equation (49) agrees well with the result obtained in Eq. (72) of Ref. [13].

IV. THERMAL CASIMIR ENERGY AND FORCE OF FERMIONIC FIELD IN A RECTANGULAR BOX

In this section, the Casimir effect at finite temperature for a massless fermionic field confined in a three-dimensional box will be calculated using the MIT bag model boundary condition. This condition allows no flux through the boundary and leads to the discrete momenta of the form [21]

$$p_i=\left(\frac{1}{2}+n_i\right)\frac{\pi}{l_i}, \quad l_1=a, l_2=b, l_3=c,$$
$$n_i=0,1,2,\ldots. \quad (50)$$

The nonrenormalized free energy for the field is defined as

$$F=F_{\rm b0}+F_T=4\sum_{n,m,j=0}\left(-\frac{1}{2}\omega_{nmj}\right)$$
$$-4T\sum_{n,m,j=0}\ln\left(1+e^{-\frac{\omega_{nmj}}{T}}\right), \quad (51)$$

where the first term $F_{\rm b0}$ is nonrenormalized energy at zero temperature, the second term F_T is the nonrenormalized thermal correction, and

$$\omega_{nmj}=\sqrt{p_1^2+p_2^2+p_3^2}$$
$$=\pi\sqrt{\frac{(n+1/2)^2}{a^2}+\frac{(m+1/2)^2}{b^2}+\frac{(j+1/2)^2}{c^2}} \quad (52)$$

are frequencies. The factor 4 appears in Eq. (51) because of the antiparticle and spin multiplicities [18]. In the following, we will compute these two terms one by one using formulas obtained in Sec. II.

The nonrenormalized energy at zero temperature had been calculated by Seyedzahedi *et al.* [21] for a cube by using a modified form of the Abel-Plana formula [35,36]

$$\sum_{n=0}g\left(n+\frac{1}{2}\right)=\int_0^\infty g(t)dt-i\int_0^\infty\frac{g(it)-g(-it)}{e^{2\pi t}+1}dt, \quad (53)$$

where $g(z)$ is analytic in the right half-plane. For arbitrary edge sizes, we can also use this formula to Eq. (51), by first performing the summation for n, then for j, and eventually for m. Eventually, one finds for the $F_{\rm b0}$ term

$$F_{\rm b0}=F_0(a,b,c)+F_{\rm f0}(a,b,c), \quad (54)$$

where

$$F_0(a,b,c)=-\left\{\frac{7\zeta(4)ac}{32\pi^2b^3}+2M_1(a,b,c)\right.$$
$$\left.+\frac{a}{b^{3/2}c^{1/2}}M_{\frac{3}{2}}\left(\frac{c}{b}\right)\right\} \quad (55)$$

is the renormalized energy at zero temperature. Here, functions $M_{3/2}(x)$ and $M_1(x,y,z)$ are defined as

$$M_1(x,y,z)=\sum_{m,k=0}\sum_{n=1}\frac{(-1)^{n+1}}{n}\sqrt{\frac{(m+1/2)^2}{y^2}+\frac{(k+1/2)^2}{z^2}}$$
$$\times K_1\left(2\pi xn\sqrt{\frac{(m+1/2)^2}{y^2}+\frac{(k+1/2)^2}{z^2}}\right), \quad (56)$$

$$M_{\frac{3}{2}}(x)=\sum_{m=0}\sum_{n=1}\frac{(-1)^{n+1}}{n^{3/2}}\left(m+\frac{1}{2}\right)^{3/2}K_{\frac{3}{2}}[2\pi(m+1/2)nx]. \quad (57)$$

Moreover,

$$F_{\rm f0}(a,b,c)=-2\pi\int_0^\infty dx\int_0^\infty dy\int_0^\infty dz\sqrt{\frac{x^2}{a^2}+\frac{y^2}{b^2}+\frac{z^2}{c^2}} \quad (58)$$

is the energy at zero temperature in the absence of the boundaries, which should be subtracted later.

The second term F_T in Eq. (51) is where our result in Sec. II, i.e., Eq. (33) will be used. As will be shown later, it is through the usage of this equation that the black-body radiation term in the free energy can be subtracted from the nonrenormalized energy to obtain a meaningful Casimir energy. Equation (33) after some tedious algebra (see Appendix A) yields the final result for F_T:

$$F_T=4TA_3(a,b,c,T)+F_{\rm fb}(a,b,c,T)-F_0(a,b,c), \quad (59)$$

where F_0 is the same as in Eq. (55) and

$$A_3(a,b,c,T)=-W_3\left(a,b,c,\frac{1}{2T}\right)-aM_1\left(c,b,\frac{1}{2T}\right)$$
$$-ac\left(\frac{2T^3}{b}\right)^{1/2}M_{\frac{3}{2}}(2bT). \quad (60)$$

Here, $M_1(x,y,z)$ and $M_{3/2}(x)$ were defined in Eqs. (56) and (57) and $W_3(x,y,z,t)$ is

$$W_3(x,y,z,t)=\sum_{m,n,k=0}\ln\left(1+e^{-2\pi x\sqrt{\frac{(m+1/2)^2}{y^2}+\frac{(n+1/2)^2}{z^2}+\frac{(k+1/2)^2}{t^2}}}\right). \quad (61)$$

The second term $F_{\rm fb}$ on the right side of Eq. (59) is found to be

$$F_{\rm fb}(a,b,c,T)=-\frac{7\zeta(4)abc}{2\pi^2}T^4. \quad (62)$$

It is easy to see that this term is indeed the free black-body radiation energy, namely, the free energy at finite temperature in the absence of boundaries

$$-4T\int_{-\infty}^\infty\frac{d^3p}{(2\pi)^3}\ln\left(1+e^{-\frac{\omega_p}{T}}\right)abc$$
$$=-\frac{7\zeta(4)abc}{2\pi^2}T^4=F_{\rm fb}(a,b,c,T). \quad (63)$$

Substituting Eqs. (54) and (59) into Eq. (51) yields the nonrenormalized free energy

$$F = 4TA_3(a,b,c,T) + F_{\rm f0}(a,b,c) + F_{\rm fb}(a,b,c,T). \quad (64)$$

To obtain the Casimir energy, the free energy in the absence of boundaries, namely, the last two terms in Eq. (64), should be subtracted from F. Thus, the final renormalized free Casimir energy is

$$F_{\rm C} = 4TA_3(a,b,c,T). \quad (65)$$

As mentioned previously, it is seen here that the removal of the thermal contribution $F_{\rm fb}(a,b,c,T)$ to the nonrenormalized energy is done by computation using Eq. (33) and correctly recognizes the continuous black-body radiation term $F_{\rm fb}(a,b,c,T)$.

It is also clear that the above Casimir free energy $F_{\rm C}$ will not depend on the order of edges a,b,c but only their sizes because the same set of $\{a,b,c\}$ always define a fixed rectangular box. We can calculate the Casimir force between any pair of opposite faces of the box. Here, we choose the pair perpendicular to edges a and then taking derivative with respect to a produces the Casimir force

$$f_a = -\frac{\partial F_{\rm C}}{\partial a} = 4T\left\{-2\pi\sum_{k,m,j=0}\frac{\sqrt{4T^2(k+1/2)^2+\frac{(m+1/2)^2}{b^2}+\frac{(j+1/2)^2}{c^2}}}{e^{2\pi a\sqrt{4T^2(k+1/2)^2+\frac{(m+1/2)^2}{b^2}+\frac{(j+1/2)^2}{c^2}}}+1} + M_1\left(c,b,\frac{1}{2T}\right) + c\left(\frac{2T^3}{b}\right)^{1/2}M_{\frac{3}{2}}(2bT)\right\}. \quad (66)$$

Let us emphasize that these are general formulas, i.e., Eqs. (65) and (66), valid for any values of lengths a,b,c and temperature T is obtained for a massless fermionic field in a three-dimensional rectangular box.

V. EFFECTS OF TEMPERATURE AND EDGE LENGTHS IN FERMIONIC CASIMIR EFFECT

With the full result of the Casimir energy (65) and force (66) for a fermionic field in a rectangular box with arbitrary sizes (a,b,c) and temperature T, we can now do a full analysis of these two quantities in the entire parameter space spanned by these four parameters.

First of all, we can reduce the full parameter space $a\in(0,\infty)\times b\in(0,\infty)\times c\in(0,\infty)\times T\in(0,\infty)$ into a smaller one by taking advantage of the cyclic symmetry of the sizes (a,b,c). That is, we will assume $b\leqslant c\leqslant a$ without losing any generality. This effectively reduces the parameter space to one-eighth of the original one. Moreover, since $1/T$ has the same dimension as length in our convention of units ($\hbar=c=\kappa_B=1$), we can directly compare it with the edge lengths. With these simplifications, we will be able to do a full analysis of the Casimir energy and force in the reduced parameter space. We will study in turn the low- and high-temperature limits, and then the finite-temperature case. In each case, we scan some ranges of the parameters and look for interesting features of the Casimir energy and force.

A. Low-temperature limit: $1/T\to\infty$

In this limit, because the only dimensional variable of the inputs are a, b, and c, the Casimir energy will depend only on one absolute scale, for which we chose b, and then the ratios between the edges. This not only means that the effective parameter space is further reduced, but also that the Casimir energy will take the form

$$F_{\rm C} = \frac{1}{b}g\left(\frac{a}{b},\frac{c}{b}\right), \quad (67)$$

where g is some function depending on a/b and c/b only. This indeed can be simply verified from Eq. (65). Therefore, without losing any generality, we can set $b=1$. There will exist three subcases: (A1) all of the edge sizes b,c,a are finite, i.e., a three-dimensional box; (A2) b,c are finite and a is infinite, i.e., a waveguide; and (A3) $b=1$ is finite and c,a are infinite, i.e., two parallel plates.

We can simply compute the zero-temperature limit of the Casimir energy and Casimir force for arbitrary edge sizes. According to Eq. (51), F_T approaches zero when T goes to zero. Hence, at zero temperature the Casimir energy (65) turns into the renormalized energy F_0 in Eq. (55)

$$F_C(a,b,c,T\to0) = F_0(a,b,c) = -\left\{\frac{7\zeta(4)ac}{32\pi^2b^3}+\frac{a}{b^{3/2}c^{1/2}}M_{\frac{3}{2}}\left(\frac{c}{b}\right) + 2M_1(a,b,c)\right\} \quad (68)$$

which is the same as (55), and by using formula (24) the Casimir force is given by

$$f_{0a}(a,b,c) = -\frac{\partial}{\partial a}F_0(a,b,c) = \frac{7\zeta(4)c}{32\pi^2b^3} + \frac{1}{b^{3/2}c^{1/2}}M_{\frac{3}{2}}\left(\frac{c}{b}\right) - \frac{2}{a}M_1(a,b,c) - 4\pi M_0(a,b,c), \quad (69)$$

where $M_{3/2}(x)$ and $M_1(x,y,z)$ were defined in Eqs. (57) and (56) and

$$M_0(x,y,z) = \sum_{m,k=0}\sum_{n=1}(-1)^{n+1}\left[\frac{\left(m+\frac{1}{2}\right)^2}{y^2}+\frac{\left(k+\frac{1}{2}\right)^2}{z^2}\right] \times K_0\left(2\pi nx\sqrt{\frac{\left(m+\frac{1}{2}\right)^2}{y^2}+\frac{\left(k+\frac{1}{2}\right)^2}{z^2}}\right). \quad (70)$$

When $b = c = a$, these equations yield the Casimir energy and Casimir force of a cube

$$F_0(a,a,a) = -\frac{1}{a}\left(\frac{7\pi^2}{2880} + 0.0142 + 0.0108\right) = -0.0489\frac{1}{a}, \tag{71}$$

$$f_{0a}(a,a,a) = \frac{1}{a^2}\left(\frac{7\pi^2}{2880} + 0.0142 - 0.0108 - 0.0437\right) = -0.0163\frac{1}{a^2}. \tag{72}$$

Our results in this special case agree perfectly with previous calculation in Eqs. (A16) of Ref. [21] done for this geometry.

For case (A1), we studied numerically the Casimir energy and force for a range of parameters using the above formulas. We plotted in Fig. 2 the Casimir energy for $b = 1$ and c from 1 to 3 and a from c to 3 and the corresponding Casimir forces along a and c directions, respectively.

It is seen that the Casimir energy is always negative while the sign of the forces in neither the a nor the c direction is fixed. The magnitude of the force in the a direction is in general smaller than that in the c direction, which is understandable because $a > c$ in this part of the parameter space. Also, because of this, the forces in both the a and c directions change much slower as a varies than they change as c varies. For the force in the a direction, as one can see from Fig. 2(b), it will change from repulsive to attractive as a decreases to almost one while c was kept a small constant $c \sim 1$. For the force in the c direction, Fig. 2(c) shows that the force also transforms from repulsive to attractive, but mainly with the decrease of c from much larger than 1 to about 1. These changes of sign of the force were also reported in Ref. [20] for parallel plates and in Ref. [37] for three-dimensional box. Lastly, the force in the b direction is independent from the forces along the a and c directions, although b itself was set to constant 1. From Fig. 2(d) it is clear that this force is always attractive in the entire range of parameters. Projecting the zero force boundary in Figs. 2(b) and 2(c) onto the parameter space spanned by (a, c), one can clearly see where the force along a, b, c directions are attractive or repulsive. One can also conclude that the force for all three pairs of opposite faces cannot be made simultaneously repulsive [37]. In region I (or IV), the force along a (or c) is repulsive while the other two directions are attractive. In region II, the force along both a, c are repulsive and that along b direction is attractive. While in region III, the force along all directions is attractive.

Equations (68) and (69) can also be used to obtain the limits in waveguide case (A2) and parallel plates case (A3). For the Casimir energy density and force density along c direction per unit length of the waveguide, we obtain

$$F_{w0}(b,c) = \lim_{a\to\infty}\frac{F_0(a,b,c)}{a} = -\left[\frac{7\zeta(4)c}{32\pi^2 b^3} + \frac{1}{b^{3/2}c^{1/2}}M_{\frac{3}{2}}\left(\frac{c}{b}\right)\right], \tag{73}$$

$$f_{w0b}(b,c) = -\frac{\partial}{\partial b}F_{w0}(b,c) = -\frac{21\zeta(4)c}{32\pi^2 b^4} + \frac{2\pi c^{1/2}}{b^{7/2}}N_{\frac{1}{2}}\left(\frac{c}{b}\right), \tag{74}$$

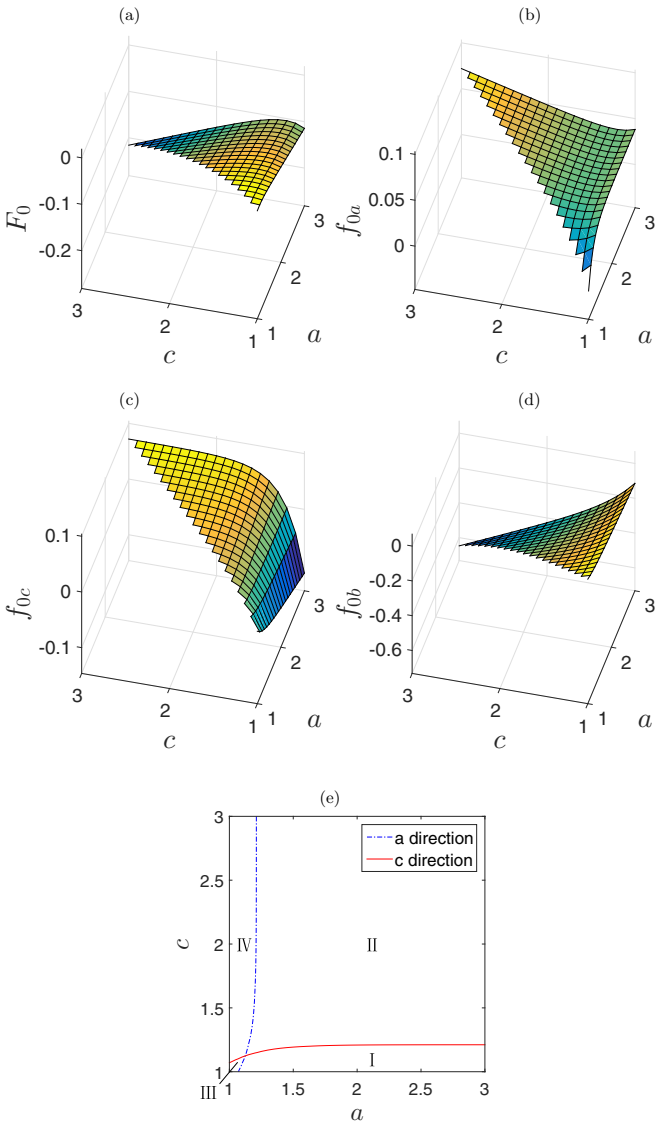

FIG. 2. (a) Casimir energy for a fermionic field in a rectangular box at zero temperature. (b)–(d) The corresponding Casimir force along b, c, and a directions, respectively. (e) The force transition boundaries. Choice of parameters are $b = 1$, c from 1 to 3, and a from c to 3. The edge sizes have a unit of an arbitrary length scale L, and consequently the Casimir energy has unit $\hbar c/L$.

where Eq. (24) has been used and

$$N_{\frac{1}{2}}(x) = \sum_{k=0}\sum_{n=1}\frac{(-1)^{n+1}}{n^{1/2}}\left(k+\frac{1}{2}\right)^{5/2}K_{\frac{1}{2}}\left[2\pi\left(k+\frac{1}{2}\right)nx\right]. \tag{75}$$

The force density along c direction takes the same form as Eq. (74) with b and c exchanged. In particular, for a waveguide with square cross section, the Casimir energy and force along the two edges are

$$F_{w0}(b,b) = -\frac{1}{b^2}\left(\frac{7\pi^2}{2880} + 0.0142\right) = -0.0382\frac{1}{b^2}, \tag{76}$$

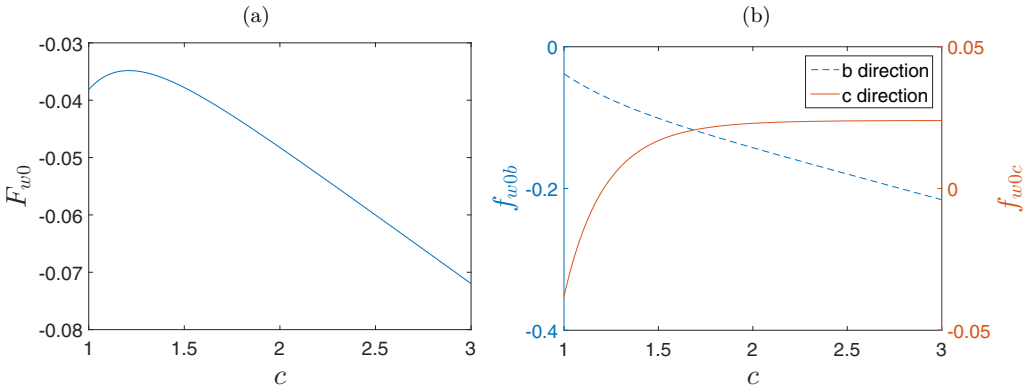

FIG. 3. (a) Casimir energy density per unit length for a fermionic field in a waveguide as the aspect ratio changes. (b) Corresponding Casimir force density along b and c directions. The edge sizes have a unit of an arbitrary length scale L, and consequently the Casimir energy has unit $\hbar c/L$.

$$f_{\mathrm{w0b}}(b,b)=\frac{1}{b^3}\left(-\frac{7\pi^2}{960}+0.0338\right)=-0.0382\frac{1}{b^3}. \quad (77)$$

For the Casimir energy and force densities per unit area of the parallel plate, we have

$$F_{\mathrm{p0}}(b)=\lim_{c\to\infty}\frac{F_{\mathrm{w0}}(b,c)}{c}=-\frac{7\pi^2}{2880b^3}, \quad (78)$$

$$f_{\mathrm{p0b}}(b)=-\frac{\partial}{\partial b}F_{\mathrm{p0}}(b)=-\frac{7\pi^2}{960b^4}. \quad (79)$$

To study in the (A2) case the effect of the aspect ratio of the waveguide cross section, we plotted in Fig. 3 the Casimir energy (73) and force (74) along b and c directions by varying the only variable c from 1 to 3 (note that $b=1$ and $a\to\infty$ already). It is seen from Fig. 3(b) that as c increases, the force in the b direction f_{w0b} is always attractive. However, in Fig. 3(a) there exists a maximal point of the Casimir energy when the ratio $r_{0\mathrm{cr}}=c/b\simeq 1.21$ which corresponds to a turning point of the force along c direction [f_{w0c} in the Fig. 3(b)]: when c is below this value, f_{w0c} was attractive and above it, f_{w0c} becomes repulsive. It is notable that Ref. [37] used the Bogoliubov transformation method and found a similar transformation but with different critical aspect ratio $r_{0\mathrm{cr}}$.

For the parallel plate case (A3), the results (78) and (79) are particularly simple. It is seen that the Casimir energy is always negative and monotonically increasing, while the force is always attractive, as anticipated from previous studies. These results are agree exactly with Refs. [18–20,37–40].

B. High-temperature limit: $1/T\to 0$

This is another case for which the effective parameter space is further reduced and therefore easier to analyze. Similar to the low-temperature limit in Sec. V A, the Casimir energy in this limit should also depend on one length scale, e.g., b, and the ratios of other edges to b. Without losing generality, therefore, we also set $b=1$.

In high temperature, however, as will be shown in Appendix B, both the Casimir energy and Casimir force approach zero:

$$\lim_{T\to\infty}F_{\mathrm{C}}=0, \quad (80)$$

$$\lim_{T\to\infty}f_a=0. \quad (81)$$

These are in alignment with the effect of high temperature, whose thermal fluctuation will suppress the quantum fluctuation that is responsible for a finite Casimir energy and force.

C. Finite-temperature case

In this case, we will use $1/T$ as the scale against which all edge sizes will be compared. For the purpose of studying Casimir energy and force, without losing any generality we can simply set $T=1$ while allowing b,c,a to vary freely in the reduced parameter space ($b\leqslant c\leqslant a$). It is also clear that we do not need to study the case that all three edges are much larger than one, which is equivalent to high-temperature case (Sec. V A), or the case that all three edges are much smaller than one, which is equivalent to the low-temperature case (Sec. V B). Taking all these into account, there are only four subcases that we need to study here: (C1) two edges a and c are much larger than $1/T$ while b is comparable or smaller than $1/T$; (C2) one edge a is much larger than $1/T$ while c and b are comparable or much smaller than $1/T$; (C3) a and c are comparable to $1/T$ while b is comparable or much smaller; and finally (C4) a is comparable to $1/T$ while c and b are much smaller.

1. Case C1

Case (C1) is equivalent, in the limit that a and c are large, to a parallel plate geometry at finite temperature. The Casimir energy and force densities per unit area in these limits are

$$F_{\mathrm{p}}(b,T)=\lim_{c\to\infty}\frac{F_{\mathrm{w}}(b,c,T)}{c}=-\frac{(2T)^{5/2}M_{\frac{3}{2}}(2bT)}{b^{1/2}}, \quad (82)$$

$$f_{\mathrm{pb}}(b,T)=-\frac{\partial}{\partial b}F_{\mathrm{p}}(b,T)$$
$$=-\frac{2(2T)^{5/2}}{b^{1/2}}\left[\frac{1}{b}M_{\frac{3}{2}}(2bT)+2\pi T N_{\frac{1}{2}}(2Tb)\right], \quad (83)$$

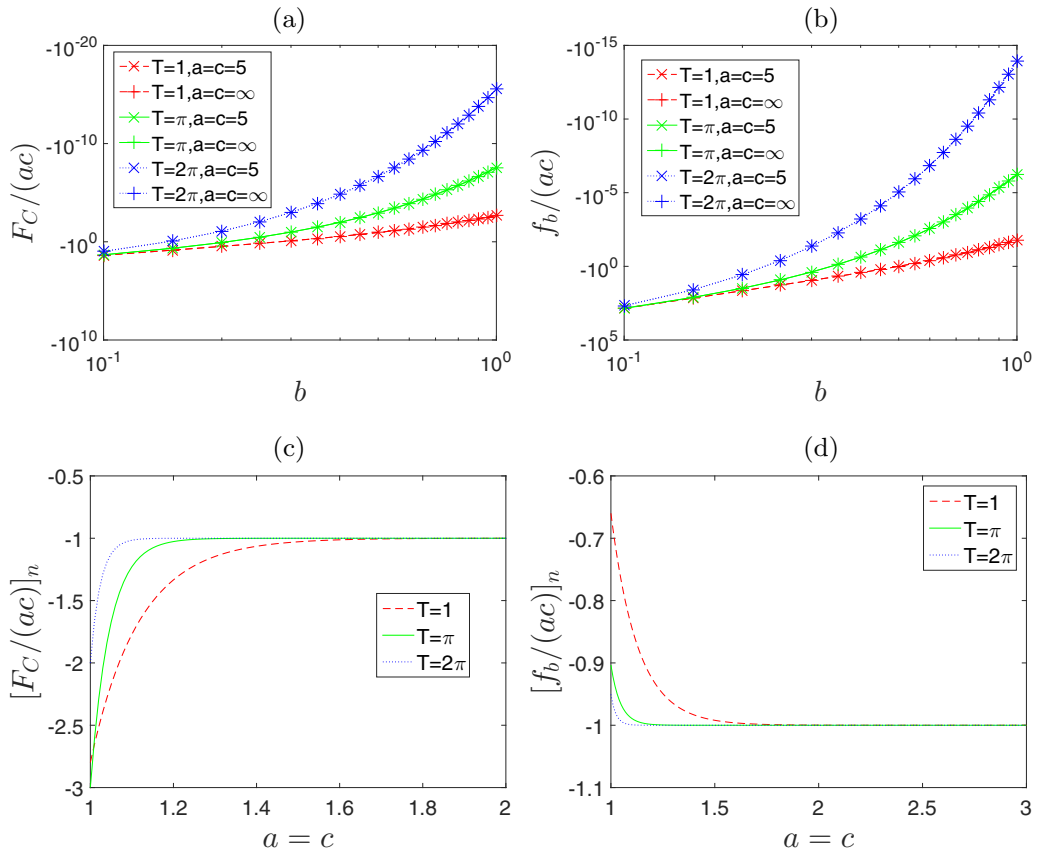

FIG. 4. (a) The Casimir energy density per unit area. (b) Casimir force density per unit area. (c) The edge-size dependence of the normalized energy density. (d) The edge-size dependence of the normalized force density. All temperatures have a unit of an arbitrary temperature scale T_A, and consequently all Casimir energies have unit $k_B T_A$ and length a, b, c have unit $\hbar c/(k_B T_A)$.

where $F_{\rm w}(b,c,T)$ is given in Eq. (84) and $N_{\frac{1}{2}}(x)$ is given in Eq. (75). We also compared these results with available literature and found that our Casimir energy density (82) agrees with Eq. (3.17) of Ref. [20] (see Appendix C) after subtracting the black-body radiation term and changing its variables $\xi \to bT$. To see more clearly the dependence of the energy and force on the plate distance and temperature, we plot in Fig. 4 in logarithmic scale the Casimir energy and force per unit area for two choices of edges $a = c = 5$ and $a = c = \infty$ and three choices of temperature $T = 1,\ \pi$, and 2π.

From Figs. 4(a) and 4(b), one sees that both the Casimir energy and force density are always negative and increase to asymptotically zero as b increases, which is expected because the plate distance increases. Note that in order to separate curves in the plots, a logarithmic scale was used in the y axis. In the linear scale, both the Casimir energy and force densities are almost a constant zero as b approaches 1. For the effect of temperature, it is seen that the higher the temperature, the faster the Casimir energy and force densities approach zero as b increases. This is in agreement with the general effect of temperature increase, which always competes with that of the quantum fluctuations responsible for Casimir energy and force and therefore suppresses them. What is remarkable here is the effect of edge sizes to the Casimir energy and force density. As can be seen from Figs. 4(a) and 4(b), the densities of both the Casimir energy and force completely coincide for $a = c = 5$ and $a = c = \infty$. Indeed, in Figs. 4(c) and 4(d) we show how the energy and force densities normalized by their asymptotic magnitudes depend on the edge sizes. It is seen from the flat tails of these plots that a box with height 1 and square top and bottom faces with edge larger than 2 has the same Casimir energy and force densities as a pair of infinitely large parallel plates with same plate distance. Moreover, the higher the temperature, the smaller the a and c need to be to resemble the asymptotic values of the Casimir force and densities. This is not surprising given that the higher temperature tends to demolish both the Casimir energy and force, as shown in the high-temperature limits in Sec. V B. This temperature effect to the Casimir energy and force densities is also observed here, although not shown in the normalized plot.

2. Case C2

Case (C2) corresponds to a waveguide geometry at high temperature compared to the waveguide's longest edge in the limit that a is large. The Casimir energy and force density along b direction per unit length in this limit are given by

$$F_{\rm w}(b,c,T) = \lim_{a\to\infty}\frac{F_{\rm C}}{a} = -4T\left[M_1\left(c,b,\frac{1}{2T}\right) + c\left(\frac{2T^3}{b}\right)^{1/2} M_{\frac{3}{2}}(2bT)\right], \tag{84}$$

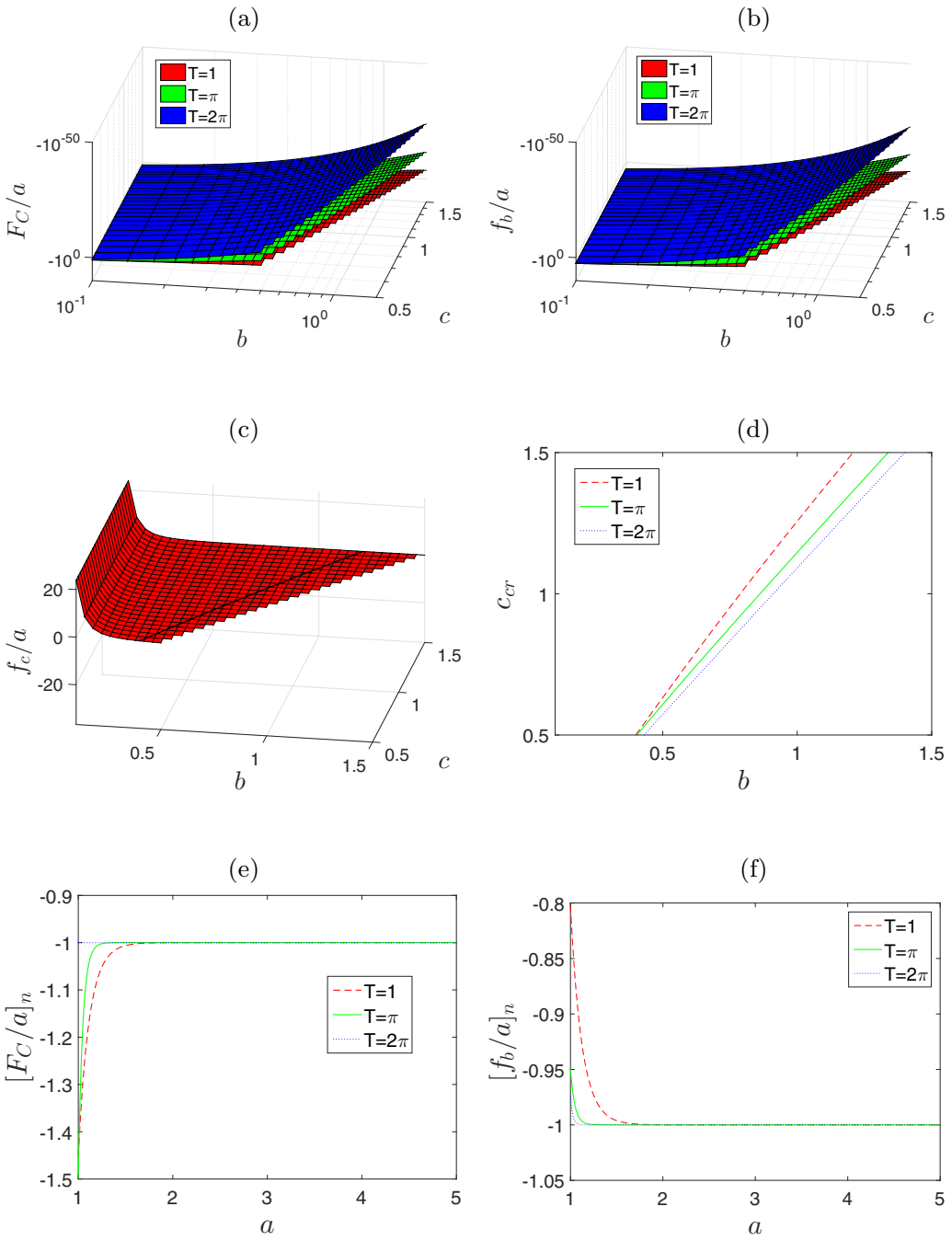

FIG. 5. (a) Casimir energy density per unit length at temperatures $T = 1, \pi, 2\pi$. (b) Casimir force density along b direction at temperatures $T = 1, \pi, 2\pi$. (c) Casimir force density along c direction at temperatures $T = 1$. (d) The critical $c_{\rm cr}$ at which the force along c direction flips sign at temperature changes. (e) The long-side edge dependence of the normalized energy. (f) The long-side edge dependence of the normalized force. We set $a = 5$. All temperatures have a unit of an arbitrary temperature scale T_A, and consequently all Casimir energies have unit $k_B T_A$ and length a, b, c have unit $\hbar c/(k_B T_A)$.

$$f_{\rm wb}(b,c,T) = -\frac{\partial}{\partial b}F_{\rm w}(b,c,T) = 8Tc\left\{\frac{\pi}{b^3}N_0\left(c,b,\frac{1}{2T}\right) - (2T^3)^{\frac{1}{2}} \times\left[\frac{1}{b^{3/2}}M_{\frac{3}{2}}(2Tb) + \frac{2\pi T}{b^{1/2}}N_{\frac{1}{2}}(2Tb)\right]\right\}. \quad (85)$$

Equation (84) is derived in Appendix C. Note that the force along c direction takes the same form as Eq. (85) but with b and c exchanged. To see clearly the edge size and temperature dependence of these quantities, we plot them in Fig. 5 for some c from smaller than 1 to comparable to 1, and b from $b \ll 1$ to c while fixing a at 5. The increase of b from $b \ll 1$ to c is equivalent to the change in the waveguide cross section from a narrow rectangular to a square.

Figure 5(a) shows that all Casimir energy densities are negative for all temperature and edge sizes. It increases monotonically as b increases in all ranges of $b \leqslant c$ and therefore the force along the b direction is always attractive, as shown in the force plot, Fig. 5(b). As c increases while keeping b fixed, however, a careful inspection shows that when b is small, $b \leqslant c_{\min} \approx 0.5$, the Casimir energy monotonically decreases. This leads to a repulsive force along the c direction. However, for larger fixed b, there exists a small interval of $c \in [b, c_{\rm cr}]$ in which the Casimir energy increases as c increases and after passing the critical $c_{\rm cr}$ the Casimir energy decreases again. This feature cannot be seen very clearly in Fig. 5(a) because of the finite element limit in it, but it is clearly shown in the c direction force density plotted in Fig. 5(c). This means that by changing the length of one side of the waveguide cross section, the nature of the Casimir force can be changed. As b increases, the critical $c_{\rm cr}$ forms a curve in this plot. Therefore, this curve is a boundary in the parameter space spanned by b and c, separating the attractive (right side of the line) and repulsive (left side of the line) forces along the c direction. We also studied how this critical boundary depends on the temperature in Fig. 5(d). It is seen that the higher the temperature, the smaller the $c_{\rm cr}$ is required for the force to flip sign.

Finally, as for the long edge-size effect, similar to the previous case of parallel plate, we found that both the Casimir energy and force densities practically gain their asymptotic value when a is as small as 2 [see Figs. 5(e) and 5(f) which show the normalized energy and force, respectively]. Besides, the value of a at which the energy and force reach their asymptotic value also decreases as temperature increases, which is the same feature as in the C1 case and understandable given high temperature suppresses the quantum fluctuation responsible for the Casimir energy and force.

3. Case C3

For case (C3), when b is much smaller than a and c, this is also equivalent to a parallel plate geometry, although the temperature here is kept low so that its inverse is comparable to the plate edge sizes. In limits that a, c are large, the Casimir energy and force have been given by Eqs. (82) and (83). As b increases, then the geometry becomes a typical rectangular box with all three edges comparable. We plotted in Fig. 6 the Casimir energy and force density per unit area for a few temperatures while keeping $a = c = 1$ and let b vary from 0.1 to 2.

It is found from Fig. 6(b) that similar to case (C1), for all temperature as long as b was smaller than a and c, the Casimir force along the b direction will always be attractive. While as b approaches a and c from below, the attractive force becomes weaker and approaches zero. After b passing $a = c = 1$, the geometry approaches a waveguide, which becomes similar to case (C2). It is also found that the force along the b direction, which is now the longer direction of the waveguide, can also change from attractive to repulsive after passing a critical $b_{\rm cr}$. We also plotted the temperature dependence of this critical

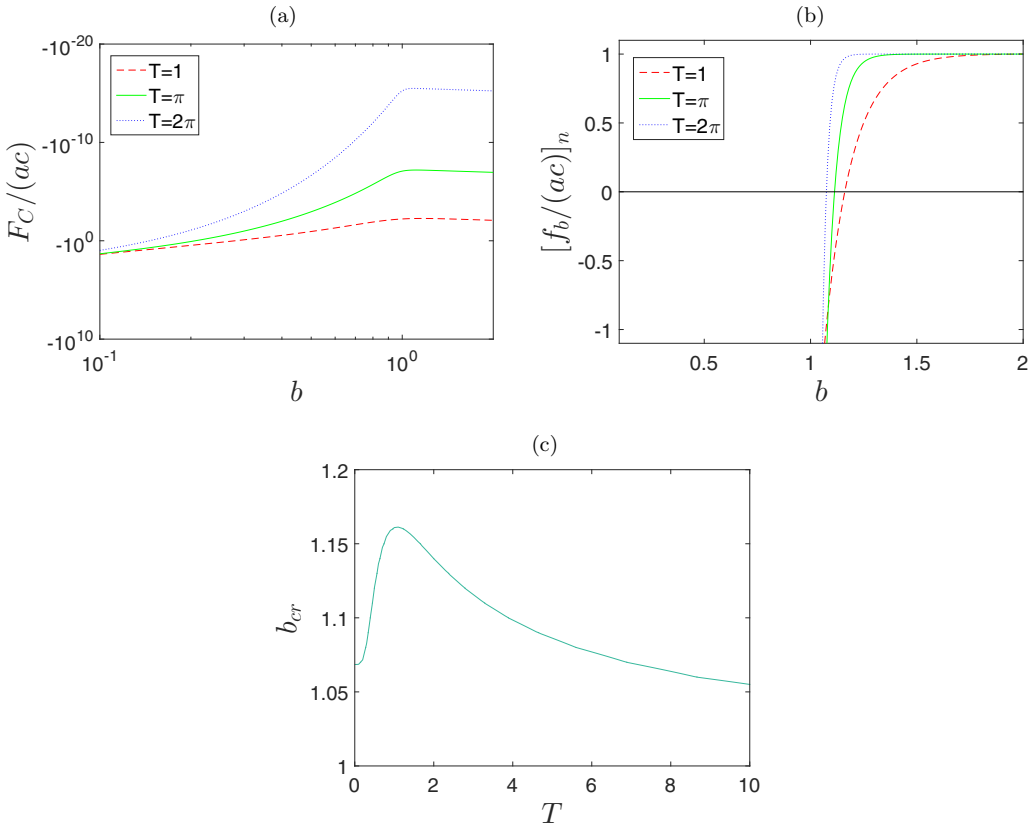

FIG. 6. (a) Casimir energy density and (b) normalized Casimir force densities using Eqs. (82) and (83) for $a = c = 1$ and b from 0.1 to 2. (c) Temperature dependence of the critical length. All temperatures have a unit of an arbitrary temperature scale T_A, and consequently all Casimir energies have unit $k_B T_A$ and length a, b, c have unit $\hbar c/(k_B T_A)$.

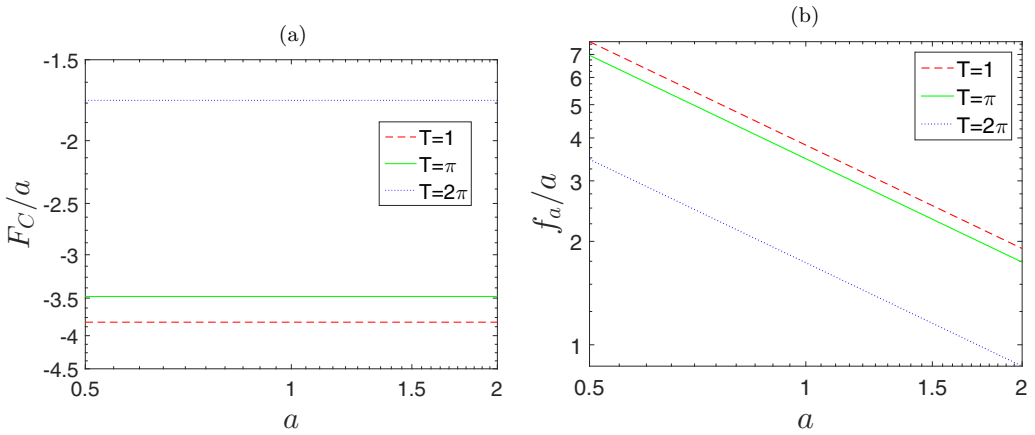

FIG. 7. (a) Casimir energy density per unit length along a direction. (b) The corresponding force density. We set $T = 1, \pi, 2\pi$ and $b = c = 0.1$. All temperatures have a unit of an arbitrary temperature scale T_A, and consequently all Casimir energies have unit $k_B T_A$ and length a, b, c have unit $\hbar c/(k_B T_A)$.

edge size in Fig. 6(c) and found that when temperature is higher than about $T = 1.1$, then similar to the critical $b_{\rm cr}$ in case (C2), the critical $b_{\rm cr}$ also decreases as the temperature increases. While for temperature below $T = 1.1$, the critical $b_{\rm cr}$ increases with the increase of temperature.

4. Case C4

For case (C4), the geometry is similar to a waveguide case but the temperature is comparable to $1/a$ which is in contrast to case (C2), and much smaller than $1/b$ or $1/c$. This also requires us to not take the $a \to \infty$ limit. We plotted in Fig. 7 the Casimir energy and force density per unit length along the a direction by setting $T = 1, \pi, 2\pi$ and $b = c = 0.1$ and varying a from $1/2$ to 2. This force density is along the longitudinal direction and analogous to the spring factor in Hooke's law. Therefore, it describes how the force factor changes with respect to the waveguide length.

It is seen from the plots that under such large length-to-width ratio, the Casimir energy exhibits an expected behavior that its density is a constant, meaning the total Casimir energy is proportional to the length. This is similar to a pair of large parallel plates in that both are proportional to the large dimension of the geometry. The foundation of this proportionality of course is that the shortest edge(s) of the rectangular box determines the density of Casimir energy, be it per unit area or per unit length. This constant energy density then means that the force density along the a direction, i.e., the force factor, decreases as $1/a^1$. This is seen in Fig. 7(b) and also easily understood from the Hooke's law.

Summarizing cases (C1)–(C4) and to get a better understanding of the transition of the Casimir force from attractive or repulsive, we combine the analysis done in the above four cases, and plot in Fig. 8 the transition surface in the parameter space spanned by all three edge sizes a, b, and c from 0.1 to 2 for temperatures $T = 1$ for the force along the a direction. It is seen that for a fixed and small a, there exists an L-shaped boundary composed mainly by two straight lines at small b and small c, respectively. In one side of the boundary where b and c are simultaneously large, the force is attractive; while on the other side of the boundary, the force is repulsive. As a increases, this L-shaped boundary also shrinks towards the larger b and c directions and eventually approaches $b, c \gtrsim 1.7$ when a reaches 2.

VI. DISCUSSIONS

The thermal Casimir energy and force for massless fermionic field confined in rectangular box are calculated in this paper. The analytic expressions are given in Eqs. (65) and (66). Their various limiting values agree with previously known results in simpler geometries. Using these results, low- and high-temperature limits and effects of finite temperature and box edge sides on the Casimir energy and force were studied. Generally, it is found that at zero temperature, there exist two boundaries (see Fig. 2) dividing the effective two-dimensional parameter space into four regions. In one of the regions, all forces along three edges are attractive, while in two other regions the force along the longest edge becomes

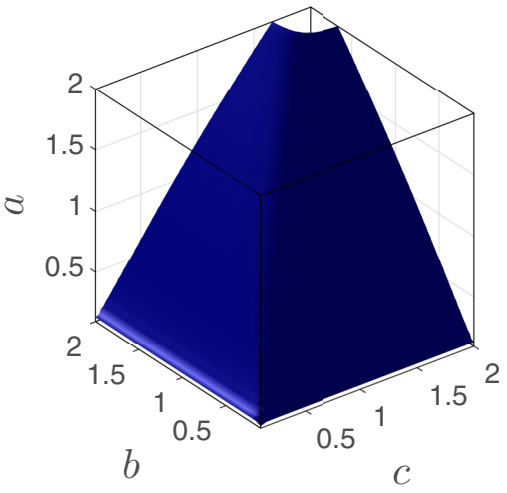

FIG. 8. Transition boundary for the force f_a from attractive to repulsive at $T = 1$. All temperatures have a unit of an arbitrary temperature scale T_A, and consequently all Casimir energies have unit $k_B T_A$ and length a, b, c have unit $\hbar c/(k_B T_A)$.

repulsive, and in the last region forces along two longest edges become positive. For the finite-temperature case, the parameter space is divided into four subcases. For a box with geometry similar to parallel plate and high temperature, the force between the plate is always attractive and becomes weaker as the plate distance or temperature increases. For the waveguide geometry at high temperature, depending on the aspect ratio of the waveguide cross section, the forces along the wider side of the cross section can transform from attractive to repulsive. The transition value of the longer cross-section edge decreases as temperature increases. For geometry of parallel plate with low temperature or geometry of box with three comparable sizes, there also exists a critical value for the longest edge length beyond which the force along this direction changes from attractive to repulsive. This critical value changes with temperature nonmonotonically. For the waveguide geometry at low temperature, as the length of the waveguide increases, the Casimir energy density per length is kept at a constant and the force density per length along the longitudinal direction decreases as length inverse. It is found that at general temperature, the parameter space of three edges can always be split by a surface into two regions according to the nature of the Casimir force along any particular direction. In the high-temperature limit, it is found that both the Casimir energy and force approaches zero.

As for the extension of this work, two possible choices might be attempted. The first is to consider other boundary conditions. Although bag model boundary conditions make the solution of the frequency modes simple, there do exist other boundary conditions [41,42], which might be more suitable for the system one wants to study. The second is to consider a massive fermionic field, which will introduce another energy scale against which the effect of temperature and edge sizes can be compared. Moreover, fermions with nonzero mass are more realistic given that the Casimir effect experiments are always carried out in condensed matter systems, in which the fermionic excitation (quasiparticles) usually has a nonzero (although sometimes small) mass. For these two directions, we expect the latter shall be easier because the former will alter the modes of the allowed quantum fluctuation and therefore affect computation in a more fundamental way.

A more dramatic turn of the future direction would be studying thermal Casimir effect of Dirac, Majorana, or Weyl fermions in a three-dimensional box. With the rise of these kinds of fermionic quasiparticles in condensed matter systems in the past years, there have also been studies of fermionic Casimir effects of them [43–45]. However, there are still a lack of studies for more complex geometry such as a three-dimensional box using these fermions with arbitrary temperature. We are currently working in this direction.

Finally, in this work we extended the Schlömilch's formula to the cases of double series and triple series. These generalized formulas can be applied to the calculation of the thermal Casimir effect for scalar field confined in rectangular boxes [13]. From this perspective, it would be appropriate to discuss relations between Schlömilch's formula and some other similar formulas, e.g., Poisson's resummation formula and Chowla-Selberg's formula [46], and their potential applications in the area of Casimir effect.

The Poisson's resummation formula describes how a general function can be expanded in a particular way. For function $f(x) = f(-x)$ and $f(x) \in L_1$, this formula is

$$\sum_{n=1}^{\infty} f(n) = -\frac{1}{2} f(0) + \int_0^{\infty} dx f(x) + 2\sum_{n=1}^{\infty} \int_0^{\infty} dx\, f(x) \cos(2\pi n x). \tag{86}$$

We now show that this formula can be directly used to prove the Schlömilch's formula (1). Indeed, using Eq. (86) to function $\frac{|x|}{e^{2\alpha|x|}-1}$ ($\alpha > 0$), one obtains

$$\begin{aligned}
&\sum_{n=1}^{\infty} \frac{n}{e^{2\alpha n}-1} \\
&= -\frac{1}{4\alpha} + \int_0^{\infty} dx \frac{x}{e^{2\alpha x}-1} \\
&\quad + 2\sum_{n=1}^{\infty} \int_0^{\infty} dx \frac{x}{e^{2\alpha x}-1} \cos(2\pi n x) \qquad (87) \\
&= -\frac{1}{4\alpha} + \frac{\pi^2}{24\alpha^2} + \sum_{n=1}^{\infty} \left[\frac{1}{4\pi^2 n^2} - \frac{\pi^2}{\alpha^2 (e^{\frac{2\pi^2 n}{\alpha}} + e^{-\frac{2\pi^2 n}{\alpha}} - 2)} \right] \\
&= -\frac{1}{4\alpha} + \frac{\pi^2}{24\alpha^2} + \frac{1}{24} - \frac{\pi^2}{\alpha^2} \sum_{n=1}^{\infty} \frac{n}{e^{\frac{2\pi^2 n}{\alpha}} - 1}, \qquad (88)
\end{aligned}$$

where formula (17) and the Abel-Plana formula (39) after setting $g(t) = t \exp(-2\pi^2 n t/\alpha)$ are used, respectively, to the first and second integrals on the right-hand side of (87). The Schlömilch's formula (1) immediately follows from Eq. (88). Because it was known that Schlömilch's formula can be used in one-dimensional Casimir effect, its derivation from Poisson's resummation formula guarantees the application of the latter in one-dimensional Casimir effect too. Using two- and three-dimensional Poisson's resummation formulas to two- and three-dimensional summations to find results similar to Eqs. (22) and (28), and analysis of the corresponding Casimir effects, however, requires a separate and large amount of work, and will not be pursued here.

The Chowla-Selberg formula was originally considered by Chowla and Selberg in Ref. [47] and then extended by Elizalde in Ref. [46, Eq. (4.32)] to carry out summation of the following form:

$$\sum_{m,n}{}' (am^2 + bmn + cn^2 + q^2)^{-s}. \tag{89}$$

This is formally similar to the double summations appearing in Eq. (38):

$$\sum_{n,m} \omega_{n,m} = \sum_{n,m} \pi \sqrt{\frac{n^2}{l_a^2} + \frac{m^2}{l_b^2}}, \tag{90}$$

where the $\omega_{n,m}$ is the energy spectrum of the electromagnetic wave confined in a two-dimensional box with sides l_a and l_b. One sees that Eq. (89) after setting $a = 1/l_b^2$, $b = 0$, $c = 1/l_a^2$, $q = 0$, and $s = -1/2$ will match Eq. (90) and, consequently, this allows us to use the extended Chowla-Selberg

formula for this double summation. This suggests that similar to the situation in Ref. [46], the extended Chowla-Selberg formula can also be applied in the calculation of Casimir effect in our case.

ACKNOWLEDGMENTS

The authors appreciate the help of M. Qin in numerical verifications of some equations. This research is supported by the National Natural Science Foundation of China Grants No. 11504276 and No. 11547310 and Ministry of Science and Technology of the People's Republic of China Grant No. 2014GB109004.

APPENDIX A: DERIVING THE EXPRESSION OF F_T

In this appendix, we show how Eq. (59) can be derived using Eq. (33) with the help of an operator $\hat{S}$ defined below. According to the definition of F_T in Eq. (51), we have

$$F_T = -4T \sum_{n,m,j=0} \ln\left(1 + e^{-\frac{\pi}{T}\sqrt{(\frac{2n+1}{2a})^2+(\frac{2m+1}{2b})^2+(\frac{2j+1}{2c})^2}}\right). \quad \text{(A1)}$$

The summations can be recast into the form

$$F_T = 4T\,\hat{S}U(a,b,c,T), \quad \text{(A2)}$$

where the operator $\hat{S}$ is defined by its action on any function $u(a,b,c)$ as

$$\begin{aligned}\hat{S}u(a,b,c) = {} & u(2a,2b,2c) + u(a,b,2c) \\ & + u(a,2b,c) + u(2a,b,c) \\ & - u(a,2b,2c) - u(2a,b,2c) \\ & - u(2a,2b,c) - u(a,b,c),\end{aligned} \quad \text{(A3)}$$

and $U(a,b,c,T)$ in Eq. (A2) is defined as

$$U(a,b,c,T) = \sum_{n,m,j=1} \ln\left(1 + e^{-\frac{\pi}{T}\sqrt{(\frac{n}{a})^2+(\frac{m}{b})^2+(\frac{j}{c})^2}}\right). \quad \text{(A4)}$$

The quantity $U(a,b,c,T)$ can be calculated by using Eq. (33) and the result is

$$\begin{aligned}U(a,b,c,T) = {} & U_1(a,b,c,T) - \left[\frac{7\zeta(4)abcT^3}{8\pi^2} + \frac{\zeta(4)ac}{16\pi^2b^3T}\right] - \frac{\pi}{T}\left[\frac{a}{4\pi b^{3/2}c^{1/2}}Y_{\frac{3}{2}}\left(\frac{c}{b}\right) + \frac{1}{2\pi}V_1(a,b,c)\right] \\ & + Z_3\left(a,b,c,\frac{1}{2T}\right) - Z_3\left(a,b,c,\frac{1}{T}\right) - aV_1\left(c,b,\frac{1}{2T}\right) + aV_1\left(c,b,\frac{1}{T}\right) \\ & - ac\left(\frac{2T^3}{b}\right)^{1/2}Y_{\frac{3}{2}}(2Tb) + \frac{ac}{2}\left(\frac{T^3}{b}\right)^{1/2}Y_{\frac{3}{2}}(Tb).\end{aligned} \quad \text{(A5)}$$

Here,

$$\begin{aligned}U_1(a,b,c,T) = {} & \frac{3\zeta(3)abT^2}{16\pi} + \frac{3\zeta(3)acT^2}{16\pi} - \frac{\pi aT}{48} + \frac{\zeta(3)a}{32\pi b^2T} + \frac{1}{2}\left[Z_2\left(\frac{1}{T},b,c\right) - Z_2\left(\frac{1}{2T},b,c\right)\right] \\ & - \frac{aTY_1(bT)}{2} + aTY_1(2bT),\end{aligned} \quad \text{(A6)}$$

$Y_{3/2}(x)$ and $V_1(x,y,z)$ were defined in Eq. (29), and $Z_3(x,y,z)$ were defined in Eq. (31).

The operator $\hat{S}$ is linear, and has the following properties when applied onto functions with one, two, or three variables with special form:

$$\begin{aligned}&\hat{S}u(a) = \hat{S}u(b) = \hat{S}u(c) = \hat{S}u(a,b) = \hat{S}u(a,c) = \hat{S}u(b,c) = 0, \\ &\hat{S}[aU(b,c)] = a[u(2b,2c) + u(b,c) - u(b,2c) - u(2b,c)], \\ &\hat{S}[acu(b)] = ac[u(2b) - u(b)].\end{aligned} \quad \text{(A7)}$$

Therefore, when it is applied to each term in $U(a,b,c,T)$ in Eq. (A5), we have

$$\hat{S}U_1(a,b,c,T) = 0, \quad \text{(A8)}$$

$$\hat{S}\left[-\frac{7\zeta(4)abcT^3}{8\pi^2} - \frac{\zeta(4)ac}{16\pi^2b^3T}\right] = -\frac{7\zeta(4)abcT^3}{8\pi^2} + \frac{7\zeta(4)ac}{128\pi^2b^3T}, \quad \text{(A9)}$$

$$\hat{S}\left[\frac{aY_{3/2}(c/b)}{b^{3/2}c^{1/2}}\right] = -\frac{a}{b^{3/2}c^{1/2}}M_{\frac{3}{2}}\left(\frac{c}{b}\right), \quad \text{(A10)}$$

$$\hat{S}V_1(a,b,c) = -M_1(a,b,c), \quad \text{(A11)}$$

$$\hat{S}\left[Z_3\left(a,b,c,\frac{1}{2T}\right) - Z_3\left(a,b,c,\frac{1}{T}\right)\right] = -W_3\left(a,b,c,\frac{1}{2T}\right), \quad \text{(A12)}$$

$$\hat{S}\left[-aV_1\left(c,b,\frac{1}{2T}\right) + aV_1\left(c,b,\frac{1}{T}\right)\right] = -aM_1\left(c,b,\frac{1}{2T}\right), \quad \text{(A13)}$$

$$\hat{S}\left[-ac\left(\frac{2T^3}{b}\right)^{1/2} Y_{\frac{3}{2}}(2Tb) + \frac{ac}{2}\left(\frac{T^3}{b}\right)^{1/2} Y_{\frac{3}{2}}(Tb)\right] = -ac\left(\frac{2T^3}{b}\right)^{1/2} M_{\frac{3}{2}}(2bT), \tag{A14}$$

where $M_{\frac{3}{2}}(x)$, $M_1(x, y, z)$, and $W_3(x, y, z, t)$ were defined in Eqs. (57), (56), and (61), respectively.

Finally, substituting them back into Eqs. (A5) and (A2) yields Eq. (59) in Sec. IV.

APPENDIX B: HIGH-TEMPERATURE LIMITS

In this appendix we first prove Eq. (46) in Sec. III. In order to do so, we only need to show that the $F_2(a, b, c, T)$ term in Eq. (43) approaches zero. Let us prove term by term that this will be zero in the high-temperature limit. When T is high enough, according to definition (31), we have

$$0 < -TZ_3\left(a, b, c, \frac{1}{2T}\right) < T\sum_{k,m,j} e^{-\pi a\sqrt{\frac{m^2}{b^2}+\frac{j^2}{c^2}+4T^2k^2}} < T\sum_{k,m,j} e^{-\pi a\frac{1}{\pi}\left(\frac{m}{b}+\frac{j}{c}+2Tk\right)}. \tag{B1}$$

Since the right side of Eq. (B1) approaches zero at high temperatures, we have

$$\lim_{T\to\infty} TZ_3\left(a, b, c, \frac{1}{2T}\right) = 0^-. \tag{B2}$$

Similarly, using definition (26) we can prove

$$\lim_{T\to\infty} TZ_2\left(x, y, \frac{1}{2T}\right) = 0^-, \quad \lim_{T\to\infty} TZ_1(2Tx) = 0^-. \tag{B3}$$

The asymptotic expression of the Bessel functions of an imaginary argument at limit $x \to \infty$ is [48]

$$K_\nu(x) = e^{-x}\sqrt{\frac{\pi}{2x}}[1 + O(x^{-1})], \quad x \to \infty. \tag{B4}$$

According to Eqs. (29) and (B4) then, when $T \to \infty$,

$$\begin{aligned} TV_1\left(c, b, \frac{1}{2T}\right) &\sim T\sum_{k,m,n} \frac{\sqrt{4T^2k^2+\frac{m^2}{b^2}}}{n}\sqrt{1\Big/\left(4nc\sqrt{4T^2k^2+\frac{m^2}{b^2}}\right)}\, e^{-2\pi cn\sqrt{4T^2k^2+\frac{m^2}{b^2}}} \\ &< T\sum_{k,m,n}\left(2Tk+\frac{m}{b}\right)e^{-2\pi cn\cdot\frac{1}{2\pi}\left(2Tk+\frac{m}{b}\right)} = T\sum_{k,m}\frac{2Tk+\frac{m}{b}}{e^{c\left(2Tk+\frac{m}{b}\right)}-1} < T\sum_{k,m}\frac{2Tk+\frac{m}{b}}{e^{c\left(2Tk+\frac{m}{b}\right)}-\frac{1}{2}e^{c\left(2Tk+\frac{m}{b}\right)}}. \end{aligned} \tag{B5}$$

It is clear then

$$\lim_{T\to\infty} TV_1\left(c, b, \frac{1}{2T}\right) = 0^+. \tag{B6}$$

According to Eqs. (23) and (B4), when $T \to \infty$,

$$T^2Y_1(2cT) \sim \sqrt{\frac{T^3}{8c}}\sum_{k,n}\sqrt{\frac{k}{n^3}}e^{-4\pi Tckn} < \sqrt{\frac{T^3}{8c}}\sum_{k,n} ke^{-4\pi Tckn} = \sqrt{\frac{T^3}{8c}}\sum_n \frac{e^{4\pi Tcn}}{(e^{4\pi Tcn}-1)^2}. \tag{B7}$$

Thus, it is also clear that the exponential term in the denominator will win over and therefore

$$\lim_{T\to\infty} T^2Y_1(2cT) = 0^+. \tag{B8}$$

According to Eq. (29) and the formula [33]

$$K_{i+1/2}(z) = \sqrt{\frac{\pi}{2z}}e^{-z}\sum_k^i \frac{(i+k)!}{k!(i-k)!(2z)^k}, \tag{B9}$$

when integer i equals 3, one can derive

$$T^{5/2}Y_{\frac{3}{2}}(2bT) = \frac{T}{2^{7/2}\pi b^{3/2}}\left[4\pi Tb\sum_n \frac{e^{4\pi Tbn}}{n^2(e^{4\pi Tbn}-1)^2} + \sum_n \frac{1}{n^3(e^{4\pi Tbn}-1)}\right]. \tag{B10}$$

Similar to the situation in Eq. (B7), hence,

$$\lim_{T\to\infty} T^{5/2}Y_{\frac{3}{2}}(2bT) = 0^+. \tag{B11}$$

Finally, combining Eqs. (B2), (B3), (B6), (B8), and (B11), it follows then

$$\lim_{T\to\infty} F_2(a,b,c,T) = 0. \tag{B12}$$

From this, Eq. (46) can be immediately obtained.

Now, let us prove Eqs. (80) and (81) in Sec. IV. For the Casimir energy, according to Eqs. (65), (60), (A10), (A11), (A12), and taking into account definition (A3), Eqs. (B2), (B6), and (B11), we can obtain very simply

$$\begin{aligned}\lim_{T\to\infty} F_{\mathrm{C}} = \lim_{T\to\infty} T A_3(a,b,c,T) = \lim_{T\to\infty} T\hat{S}\Big\{ & Z_3\Big(a,b,c,\frac{1}{2T}\Big) - Z_3\Big(a,b,c,\frac{1}{T}\Big) - aV_1\Big(c,b,\frac{1}{2T}\Big) \\ & + aV_1\Big(c,b,\frac{1}{T}\Big) - ac\Big(\frac{2T^3}{b}\Big)^{1/2} Y_{\frac{3}{2}}(2Tb) + \frac{ac}{2}\Big(\frac{T^3}{b}\Big)^{1/2} Y_{\frac{3}{2}}(Tb)\Big\} = 0,\end{aligned} \tag{B13}$$

which is Eq. (80).

For the Casimir force, denoting the first term of Eq. (66) by f_1, it is clear that in the first term the exponential term in the denominator dominates the numerators

$$\lim_{T\to\infty} f_1 = 0^-. \tag{B14}$$

According to Eqs. (A13) and (B6), (A14) and (B11), and the definition of $\hat{S}$ in Eq. (A3), one finds

$$\lim_{T\to\infty} T M_1\Big(c,b,\frac{1}{2T}\Big) = \lim_{T\to\infty} T^{\frac{5}{2}} M_{\frac{3}{2}}(2Tb) = 0. \tag{B15}$$

Combination of Eqs. (B14) and (B15) proves Eq. (81) in Sec. IV.

APPENDIX C: WAVEGUIDE AND PARALLEL PLATE LIMITS

In this appendix we derive the formula for the Casimir energy per unit length in the case of waveguide and per unit area in the case of parallel plate, i.e., Eqs. (84) and (82). For the waveguide case, from definitions (65), (60), and (61), it is seen that in order to prove Eq. (84), we need to study the limits $\lim_{a\to\infty} W_3(a,b,c,x)/a$. Similar to the argument from Eq. (B1) to Eq. (B2), one can obtain

$$\lim_{a\to\infty} \frac{1}{a} W_3\Big(a,b,c,\frac{1}{2T}\Big) = 0. \tag{C1}$$

Using this, Eq. (84) immediately follows.

In order to further prove Eq. (82), we need to study the limit of $\lim_{c\to\infty} M_1(c,x,y)/c$. Similar to the argument from Eq. (B4) to Eq. (B6), one can obtain

$$\lim_{a\to\infty} \frac{1}{a} V_1(a,b,c) = 0, \tag{C2}$$

Then, according to Eq. (A11) and definition of $\hat{S}$ in Eq. (A3), Eq. (C2) further implies

$$\lim_{a\to\infty} \frac{1}{a} M_1(a,b,c) = 0. \tag{C3}$$

Using this equation and Eq. (84), Eq. (82) follows.

Lastly, let us show that after subtracting from Eq. (3.17) of Ref. [20] a free black-body radiation energy term, the free Casimir energy will agree with our result (C3). We will do the proof backward. First, letting $\xi = bT$ and defining

$$g(\xi) = b^3 F_p(b,T), \tag{C4}$$

then according to Eqs. (82), (57), and (B9) this Casimir energy becomes

$$\begin{aligned} g(\xi) &= -(2\xi)^{5/2} M_{\frac{3}{2}}(2\xi) = \frac{\xi}{4\pi}\sum_n \frac{(-1)^n[\sinh(2\pi\xi n) + 2\pi\xi n\,\cosh(2\pi\xi n)]}{n^3\,\sinh^2(2\pi\xi n)} \\ &= \frac{\xi}{4\pi}\Big\{\sum_n \frac{2[\sinh(4\pi\xi n) + 4\pi\xi n\,\cosh(4\pi\xi n)]}{(2n)^3\sinh^2(4\pi\xi n)} - \sum_n \frac{\sinh(2\pi\xi n) + 2\pi\xi n\,\cosh(2\pi\xi n)}{n^3\sinh^2(2\pi\xi n)}\Big\} \\ &= -\frac{\xi^3}{16\pi}\frac{\partial}{\partial\xi}\frac{1}{\xi}\sum_n \frac{1}{n^3}\Big(\frac{1}{\sinh(4\pi n\xi)} - \frac{4}{\sinh(2\pi n\xi)}\Big). \end{aligned} \tag{C5}$$

Clearly, this is different from the dimensionless free energy $f(\xi)$ in Eq. (3.17) of Ref. [20] by just the black-body radiation term given in the square brackets below:

$$g(\xi) = f(\xi) - \left[-\frac{7\pi^2\xi^4}{180}\right]. \tag{C6}$$

[1] H. B. G. Casimir, Indag. Math. **10**, 261 (1948); Front. Phys. **65**, 342 (1987).
[2] M. J. Sparnaay, Physica (Amsterdam) **24**, 751 (1958).
[3] W. Arnold, S. Hunklinger, and K. Dransfeld, Phys. Rev. B **19**, 6049 (1979).
[4] S. K. Lamoreaux, Phys. Rev. Lett. **78**, 5 (1997); **81**, 5475(E) (1998).
[5] U. Mohideen and A. Roy, Phys. Rev. Lett. **81**, 4549 (1998).
[6] T. H. Boyer, Phys. Rev. **174**, 1764 (1968).
[7] K. A. Milton, L. L. DeRaad, Jr., and J. S. Schwinger, Ann. Phys. (NY) **115**, 388 (1978).
[8] E. M. Lifshitz, Zh. Eksp. Teor. Fiz. **29**, 94 (1955) [Sov. Phys.–JETP **2**, 73 (1956)].
[9] J. Ambjørn and S. Wolfram, Ann. Phys. **147**, 1 (1983).
[10] F. C. Santos and A. C. Tort, Phys. Lett. B **482**, 323 (2000).
[11] R. Jáuregui, C. Villarreal, and S. Hacyan, Ann. Phys. **321**, 2156 (2006).
[12] S. C. Lim and L. P. Teo, J. Phys. A: Math. Gen. **40**, 11645 (2007).
[13] B. Geyer, G. L. Klimchitskaya, and V. M. Mostepanenko, Eur. Phys. J. C **57**, 823 (2008).
[14] S. C. Lim and L. P. Teo, Eur. Phys. J. C **60**, 323 (2009).
[15] S. C. Lim and L. P. Teo, New J. Phys. **11**, 013055 (2009).
[16] R. H. Lin and X. H. Zhai, Int. J. Mod. Phys. A **29**, 1450043 (2014).
[17] R. Balian and B. Duplantier, Ann. Phys. **112**, 165 (1978).
[18] K. Johnson, Acta Phys. Polon. B **6**, 865 (1975).
[19] P. W. Milonni, *The Quantum Vacuum: An Introduction to Quantum Electrodynamics* (Academic, Boston, 1994).
[20] S. A. Gundersen and F. Ravndal, Ann. Phys. **182**, 90 (1988).
[21] A. Seyedzahedi, R. Saghian, and S. S. Gousheh, Phys. Rev. A **82**, 032517 (2010).
[22] K. A. Milton, *The Casimir Effect: Physical Manifestations of Zero-Point Energy* (World Scientific, River Edge, 2001).
[23] H. Sukamto and A. Purwanto, J. Mod. Phys. **4**, 597 (2013).
[24] O. Schlömilch, Ber. Verh. K. Sachs. Gesell. Wiss. Leipzig **29**, 101 (1877).
[25] O. Schlömilch, *Compendium der Höheren Analysis*, 4th ed., Vol. 2 (Friedrich Vieweg und Sohn, Braunschweig, 1895).
[26] J. Lagrange, Bull. Sci. Math. **84**, 105 (1960).
[27] E. Grosswald, Acta Arith. **21**, 25 (1972).
[28] J. S. Dowker and K. Kirsten, Nucl. Phys. B **638**, 405 (2002).
[29] B. C. Berndt, *Ramanujan' s Notebooks, Part II* (Springer, New York, 1989).
[30] M. Planck, Ann. Phys. **4**, 553 (1901).
[31] R. P. Feynman, *Statistical Mechanics: A Set of Lectures* (Benjamin/Cummings, Massachusetts, 1972).
[32] Z. X. Wang and D. R. Guo, *Special Functions* (World Scientific, Singapore, 1989).
[33] I. S. Gradshteyn and I. M. Ryzhik, *Table of Integrals, Series, and Products*, 7th ed., edited by A. Jeffrey and D. Zwillinger (Academic, New York, 2007).
[34] V. M. Mostepanenko and N. N. Trunov, *The Casimir Effect and Its Applications* (Clarendon, Oxford, 1997).
[35] M. Bordag, U. Mohideen, and V. M. Mostepanenko, Phys. Rep. **353**, 1 (2001).
[36] A. A. Saharian, arXiv:0708.1187.
[37] H. Queiroz, J. C. da Silva, F. C. Khanna, J. M. C. Malbouisson, M. Revzen, and A. E. Santana, Ann. Phys. **317**, 220 (2005); **321**, 1274(E) (2006).
[38] C. D. Fosco and E. L. Losada, Phys. Rev. D **78**, 025017 (2008).
[39] V. M. Mostepanenko and N. N. Trunov, Sov. Phys.–Usp. **31**, 965 (1988).
[40] F. C. Santos and A. C. Tort, arXiv:quant-ph/0201104.
[41] X. H. Zhai, X. Z. Li, and C. J. Feng, Eur. Phys. J. C **71**, 1654 (2011).
[42] E. Elizalde, S. D. Odintsov, and A. A. Saharian, Phys. Rev. D **83**, 105023 (2011).
[43] A. V. Shytov, D. A. Abanin, and L. S. Levitov, Phys. Rev. Lett. **103**, 016806 (2009).
[44] E. R. Bezerra de Mello, F. Moraes and A. A. Saharian, Phys. Rev. D **85**, 045016 (2012).
[45] S. LeBohec, J. Talbot, and E. G. Mishchenko, Phys. Rev. B **89**, 045433 (2014).
[46] E. Elizalde, *Ten Physical Applications of Spectral Zeta Functions* (Springer, Berlin, 1995).
[47] S. Chowla and A. Selberg, Proc. Natl. Acad. Sci. U. S. A. **35**, 371 (1949).
[48] D. J. Maširević, Integral Transforms Spec. Funct. **26**, 273 (2015).